

CHAPTER 3

RESULTS AND DISCUSSION

3.1 Synthesis of water-soluble cationic sexithiophenes: 6TNL and 6TND

In this study, two types of water-soluble cationic sexithiophenes, 6TNL and 6TND, were synthesized and characterized. The main difference of these sexithiophenes based on the conjugation linkage of thiophene units in the molecules. The linear sexithiophene (6TNL) has only α,α -linkage whereas 6TND has both α,α - and α,β -linkages. The well-known Stille coupling reaction which is the one of the two most general organic synthetic methods was used for the formation of new C-C bonds between thiophene units. This synthetic method offers the efficient C-C bond formation for various heterocycles such as thiophenes [116]. The reaction is useful for modern synthesis due to its ease to perform even though the reaction is very sensitive to oxygen. This harmful oxygen, however, can be easily removed by using the several freeze-thaw cycles. The freeze-thaw cycle is the procedure that material is frozen under nitrogen gas and then thawed to room temperature. The material is subsequently performed under vacuum and then repeated until the desired cycles are reached.

As shown in Figure 2.1 (page 50), the 5-(6-bromo-hexyl)-[2,2']bithiophenyl (**1**) was synthesized from commercial bithiophene by monolithiation, followed by the reaction with 1,6-dibromohexane. The obtained product was then brominated at the remained α -position of thiophene unit with NBS, followed by the Stille coupling reaction with 2,5'-bis-(tributylstannyl)-2,2'-bithiophene. The 6TNL was achieved by heating this

compound with excess amount of trimethylamine in ethanol until the reaction was complete. The synthetic procedure was also previously reported by Advincula group [50].

The synthetic scheme for 6TND is shown in Figure 2.2 (page 83). The key starting material for this sexithiophene is 2,3-dibromothiophene which is commercially available material. The new C-C bond can be formed through the Stille coupling of C-Br group at 2,3 positions of 2,3-dibromothiophene and 5 position of tributyltin derivative. The direct coupling of this obtained product (**7**) through $\text{CuCl}_2/n\text{-BuLi}$ was used to synthesize the sexithiophene (**8**). However, this coupling reaction was not efficient affording very low yield. The cleavage of terminated alkyl methoxide group of (**8**) to bromide group was performed using aqueous hydrogen bromide solution. Finally, the same procedure for synthesis of 6TNL was followed to synthesize 6TND.

As mentioned in Chapter 1, the introduction of hexyl substituents to α -position of thiophene units produced the soluble sexithiophene in various organic solvents [27]. In this study, the introduction of quaternary ammonium group to the synthesized sexithiophenes provided the water-soluble sexithiophenes. The introduction of hexyl methoxide group has more advantages than the introduction of hexyl one. The introduction of hexyl methoxide group makes the separation easier due to the bigger difference in polarity between starting materials and the obtained products. Moreover, the hexyl methoxide group serves as the precursor/protecting group for alkyl bromide group. It easily cleaves in acid but it is stable under basic condition. The other possible reason is that methoxide group is the smallest protecting group available for bromide group [57].

Table 3.1 Percent yield for the synthesis of 6TNL, 6TND and PCEMMA

Product	Actual weight (g)	Yield (%)
5-(6-bromo-hexyl)-[2,2']bithiophenyl (1)	13.0	50.0%
5'-bromo-5-(6-bromo-hexyl)-2,2'-bithiophene (2)	4.30	81.0%
2,5'-bis-(6-bromohexyl)sexithiophene (3)	1.70	83.0%
6TNL	0.50	85.0%
1-bromo-6-methoxyhexane (4)	42.0	53.8%
2-(6-methoxyhexyl)thiophene (5)	20.5	37.3%
2,3-bis(5-(6-methoxyhexyl)thiophen-2-yl)thiophene (7)	7.65	42.2%
5-(4,5-bis(5-(6-methoxyhexyl)thiophen-2-yl)thiophen-2-yl)-2,3-bis(5-(6-methoxyhexyl)thiophen-2-yl)thiophene (8)	0.230	7.69 %
5-(4,5-bis(5-(6-bromohexyl)thiophen-2-yl)thiophen-2-yl)-2,3-bis(5-(6-bromohexyl)thiophen-2-yl)thiophene (9)	0.160	57.7 %
6TND	0.192	99.0%
2-(<i>N</i> -carbazolyl)ethyl methacrylate (10)	8.30	62.8%
PCEMMA		75.0%

All synthesized compounds were characterized by using NMR technique which will be reported in the next topic. The expanded $^1\text{H-NMR}$ spectra showed the differences between the starting materials and the obtained products. The calculated chemical shift was obtained by using ChemDraw® Ultra 8.0.3 program (©CambridgeSoft Corporation, USA). The raw NMR data were processed by using NutsPro-NMR Utility Transform Software-Professional (©Acron NMR, USA). Moreover, 6TND was further characterized by using LC-MS technique. The technique was used to confirm the complete substitution for all 4 positions of bromide by quaternary ammonium group. The obtained yields of the products are shown in Table 3.1.

3.2 Synthesis of water-soluble anionic polycarbazole precursor: PCEMMA

The water-soluble anionic polycarbazole precursor, PCEMMA, was synthesized and characterized. The synthesis procedure involved with the partial esterification or copolymerization of acrylic acid and acrylic ester to form polyacrylate and polyacrylic acid copolymer. The synthesis scheme is previously shown in Figure 2.3 (page 88). The acrylic ester monomer containing electrochemical active carbazole as pendant group was synthesized from the reaction of methacrylic acid and 9*H*-Carbazole-9-ethanol in DCC/DMAP. The introduction of carbazole group utilized the ability for electrochemical synthesis of polycarbazole network on solid substrates.

The synthesized compounds were characterized by using NMR technique. Moreover, PCEMMA was characterized by using elemental analysis to investigate the ratio content of acrylate and acrylic acid units. It was found that the actual ratio of

acrylate and acrylic acid was 3:2 with the monomer feed ratio of 1:1. The elemental analysis data is shown in Table 3.2. The found percentage of each element were obtained from CHNS/O analysis. The calculated percentage of each element can be obtained using NutsPro-NMR Utility Transform Software-Professional (©Acron NMR, USA). The obtained polymer was also characterized by using gel permeation chromatography (GPC) technique which is the technique used for determination of average molecular weight of material. The weight-average molecular weight (\bar{M}_w) and number-average molecular weight (\bar{M}_n) were 2,933 and 1,083 respectively. The obtained polymer was slightly soluble in water which showed greater solubility when adding DMSO in the ratio of 2:3 v/v (DMSO: water) at pH 10.

Table 3.2 Elemental analysis data of PCEMMA

Element	Found (%)	Calculated (%)
C	72.56	72.89
H	6.40	7.39
N	4.36	3.54
O	16.68	16.18

3.3 Characterization of water-soluble cationic linear sexithiophene: 6TNL

3.3.1 Characterization of 5-(6-bromo-hexyl)-[2,2']bithiophenyl

The $^1\text{H-NMR}$ data of 5-(6-bromo-hexyl)-[2,2']bithiophenyl is shown in Table 3.3 and the $^1\text{H-NMR}$ spectrum is shown in Figure 3.1.

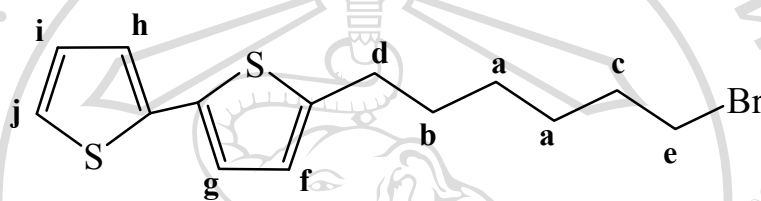


Table 3.3 $^1\text{H-NMR}$ data of 5-(6-bromo-hexyl)-[2,2']bithiophenyl

^1H position	Chemical shift (ppm)	Calculated chemical shift (ppm)
a	1.38-1.49	1.29
b	1.62-1.72	1.62
c	1.81-1.90	1.79
d	2.75-2.80	2.55
e	3.38-3.43	3.30
f	6.65-6.68	6.60
g,h	6.89-6.92	6.70-7.00
i,j	7.09-7.11	7.00, 7.20

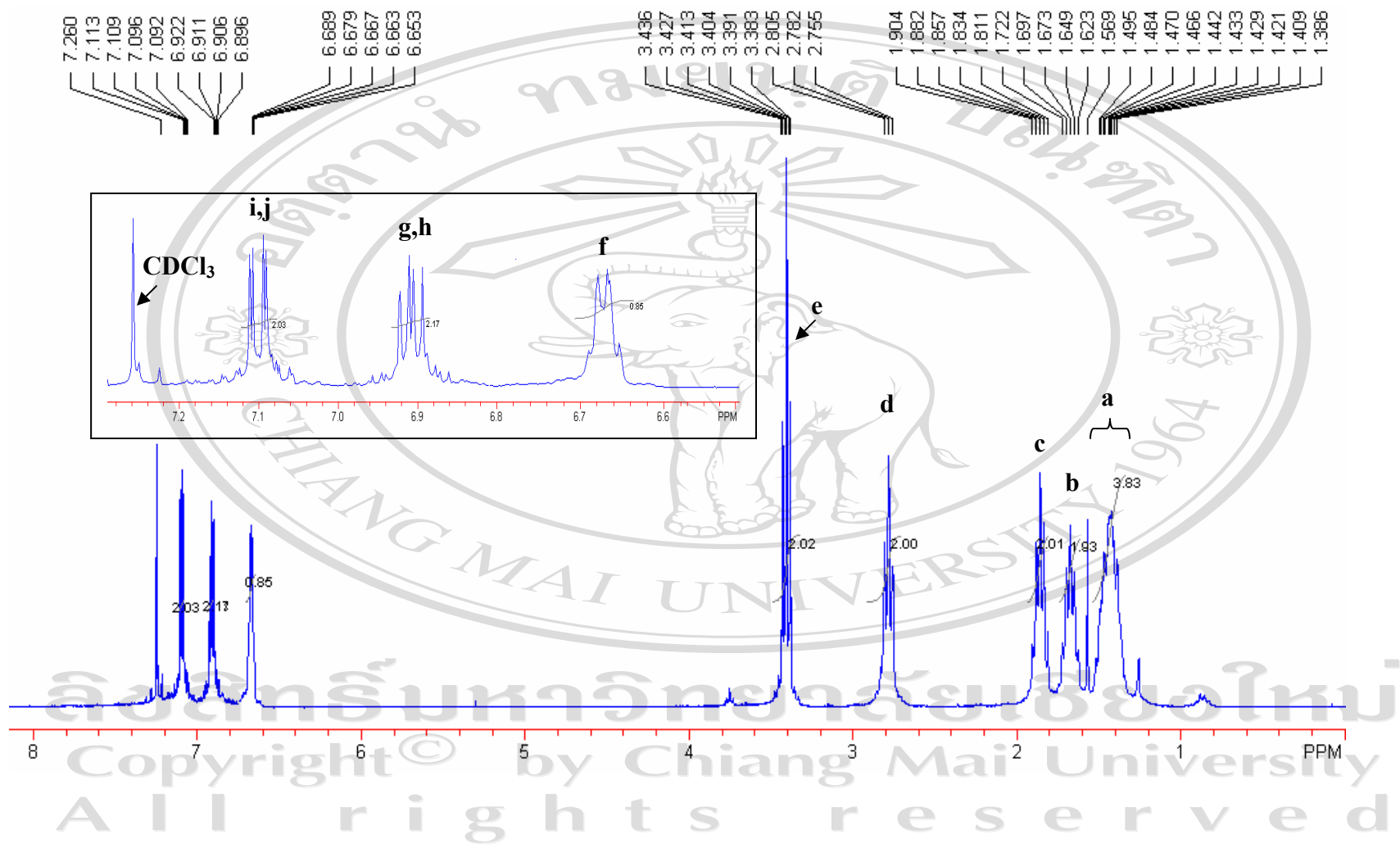


Figure 3.1 $^1\text{H-NMR}$ spectrum of 5-(6-bromo-hexyl)-[2,2']bithiophenyl in CDCl_3

3.3.2 Characterization of 5'-bromo-5-(6-bromohexyl)-2,2'-bithiophene

The $^1\text{H-NMR}$ data of 5'-bromo-5-(6-bromohexyl)-2,2'-bithiophene is shown in Table 3.4 and the $^1\text{H-NMR}$ spectrum is shown in Figure 3.2.

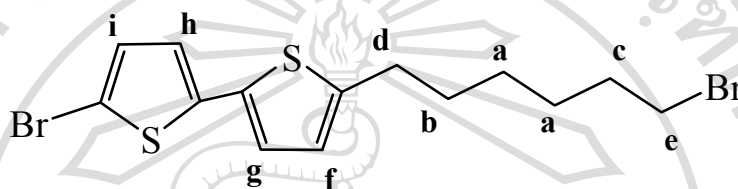


Table 3.4 $^1\text{H-NMR}$ data of 5'-bromo-5-(6-bromo-hexyl)-2,2'-bithiophene

^1H position	Chemical shift (ppm)	Calculated chemical shift (ppm)
a	1.38-1.49	1.29
b	1.62-1.72	1.62
c	1.81-1.90	1.79
d	2.75-2.80	2.55
e	3.38-3.47	3.30
f,g	6.86-6.89	6.60, 6.70
h,i	6.94-6.95	6.70, 6.90

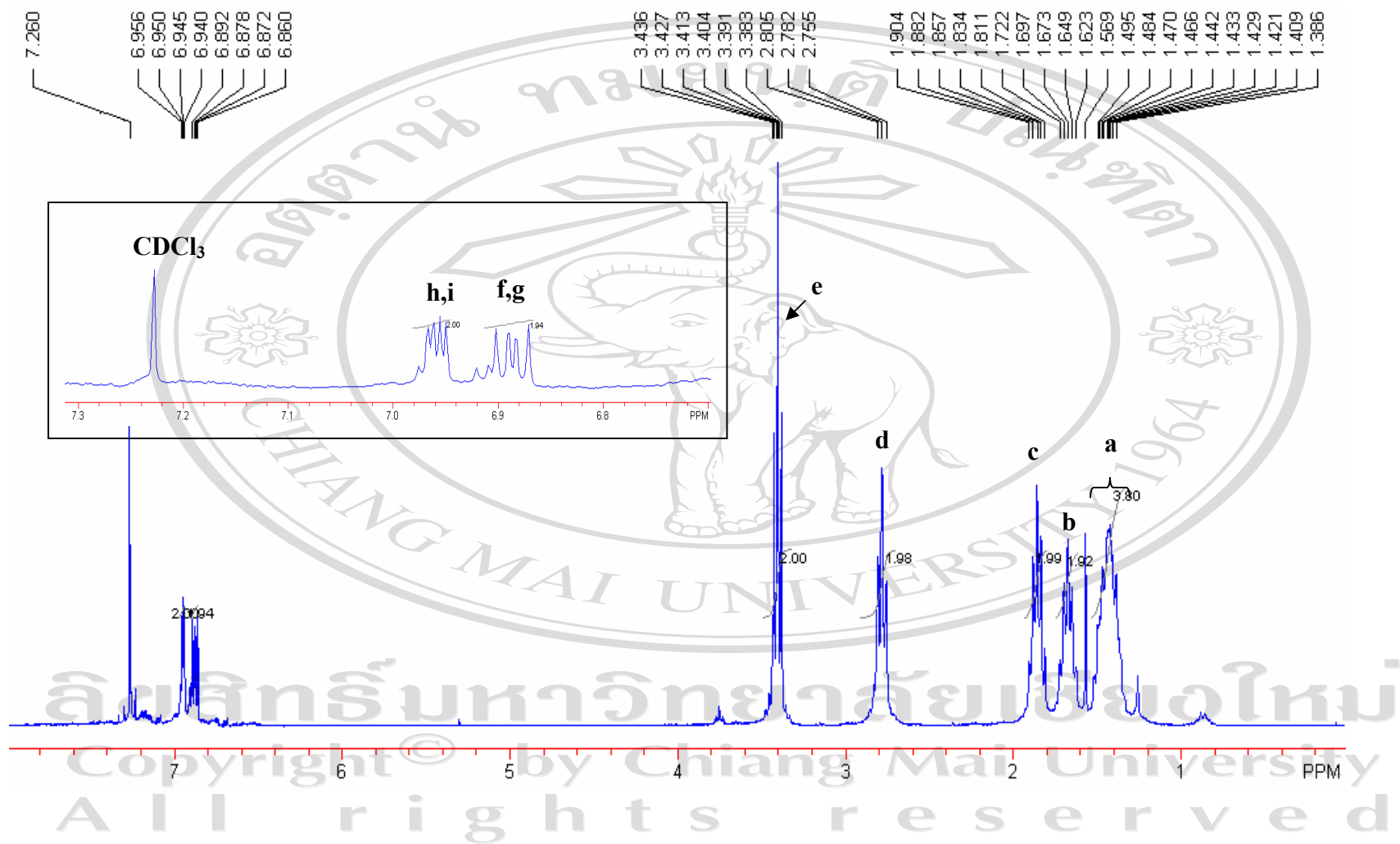


Figure 3.2 ¹H-NMR data of 5'-bromo-5-(6-bromohexyl)-2,2'-bithiophene in CDCl₃

3.3.3 Characterization of 2,5'-bis-(6-bromohexyl)sexithiophene

The $^1\text{H-NMR}$ data of 2,5'-bis-(6-bromohexyl)sexithiophene is shown in Table 3.5 and the $^1\text{H-NMR}$ spectrum is shown in Figure 3.3.

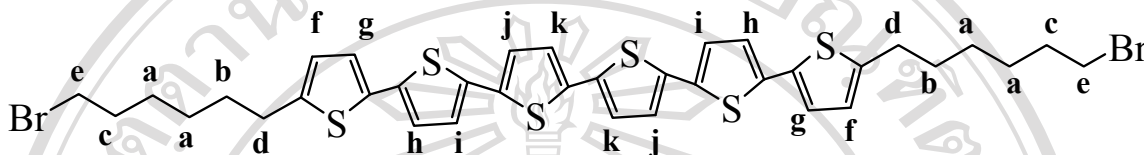


Table 3.5 $^1\text{H-NMR}$ data of 2,5'-bis-(6-bromohexyl)sexithiophene

^1H position	Chemical shift (ppm)	Calculated chemical shift (ppm)
a	1.39-1.52	1.29
b	1.59-1.70	1.62
c	1.82-1.91	1.79
d	2.81-2.86	2.55
e	3.41-3.46	3.30
f,g	6.69-6.71	6.6,6.7
h,i	6.97-7.00	7.0,7.0
j,k	7.03-7.04	7.0,7.0

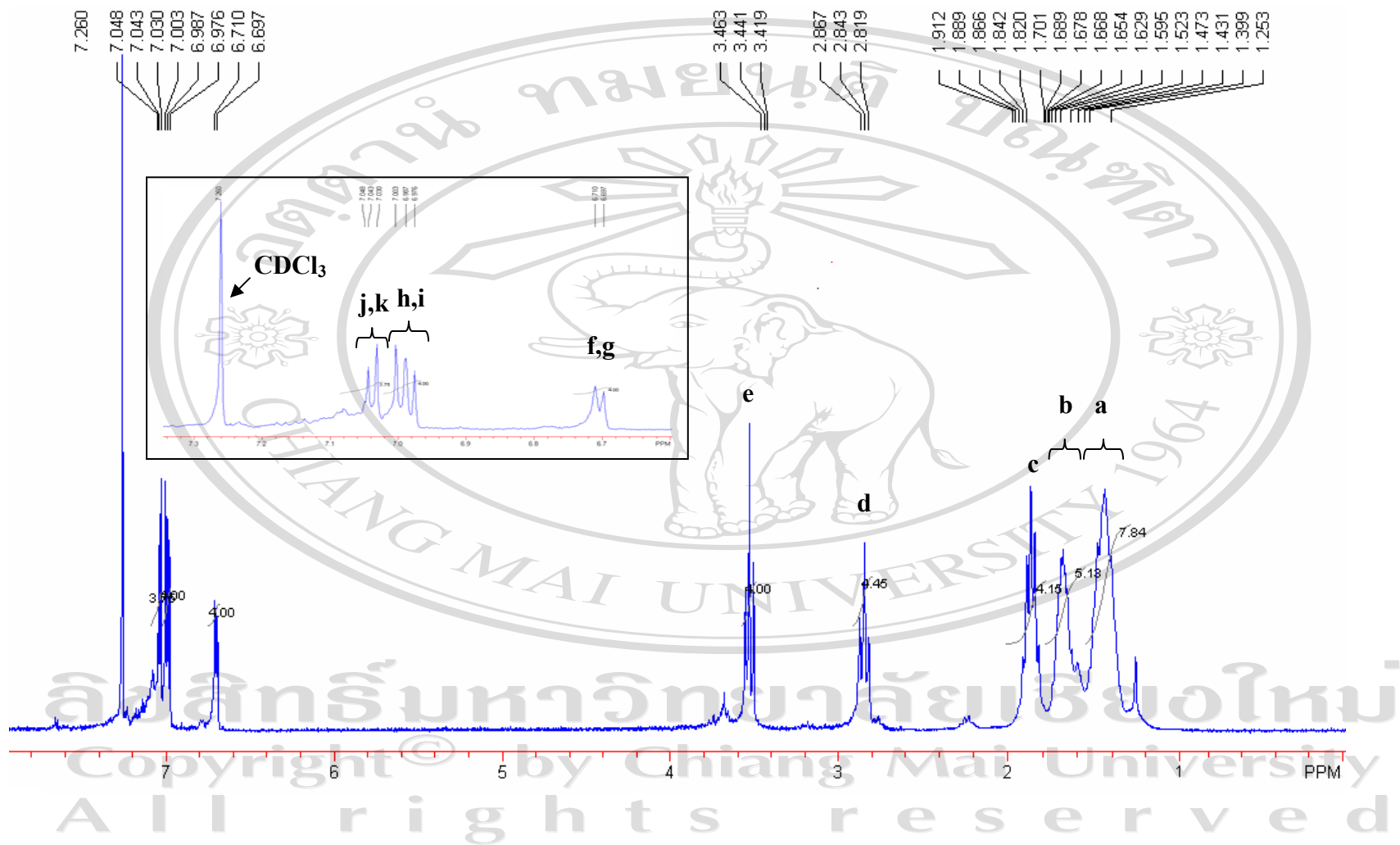


Figure 3.3 ¹H-NMR spectrum of 2,5'-bis-(6-bromohexyl)sexithiophene in CDCl₃

3.3.4 Characterization of 6TNL

The $^1\text{H-NMR}$ data of 6TNL is shown in Table 3.6 and the $^1\text{H-NMR}$ spectrum is shown in Figure 3.4.

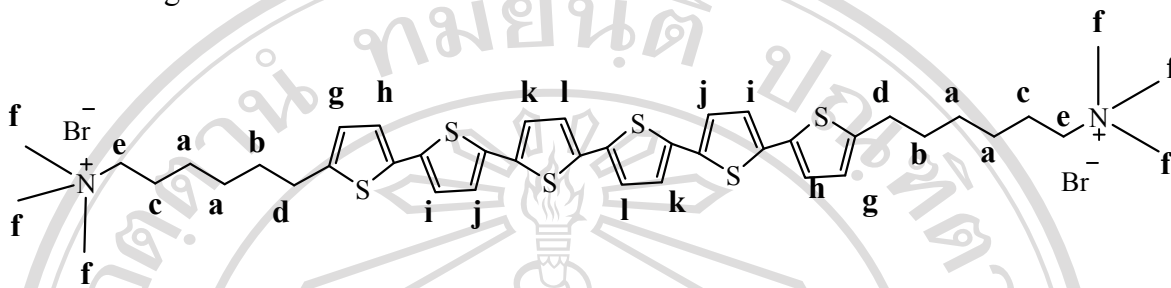


Table 3.6 $^1\text{H-NMR}$ data of 6TNL

^1H position	Chemical shift (ppm)	Calculated chemical shift (ppm)
a	1.39-1.52	1.29
b	1.59-1.70	1.62
c	1.82-1.91	1.73
d	2.78-2.95	2.55
e	3.39-3.45	3.24
f	3.18	3.30
g	6.69-6.70	6.60
h,i,j	6.97-7.03	6.70
k	7.05-7.06	7.00
l	7.15-7.20	7.00

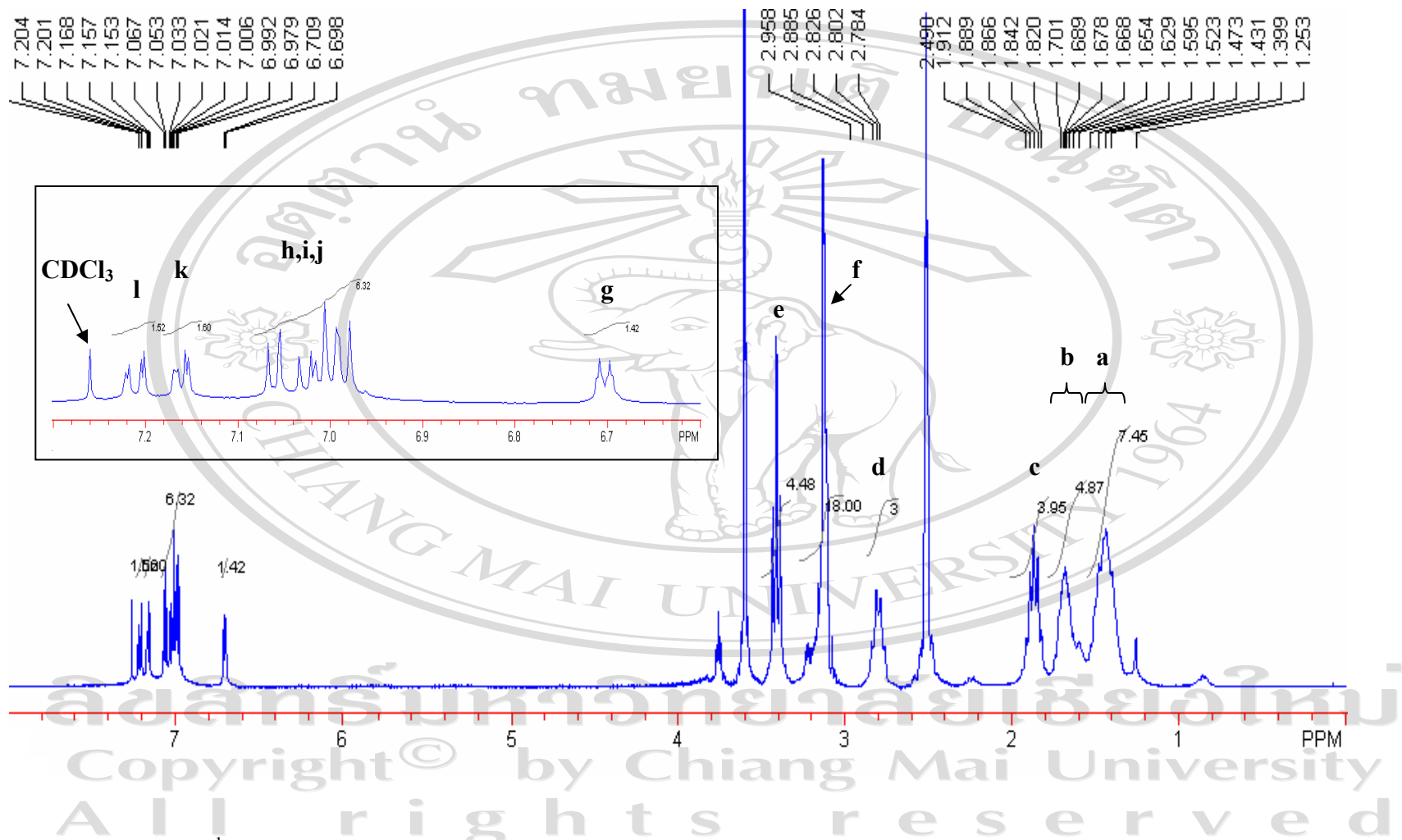


Figure 3.4 ¹H-NMR spectrum of 6TNL in deuterated DMSO

3.4 Characterization of water-soluble cationic dendrimeric sexithiophene: 6TND

3.4.1 Characterization of 1-bromo-6-methoxyhexane

The $^1\text{H-NMR}$ data of 1-bromo-6-methoxyhexane is shown in Table 3.7 and the $^1\text{H-NMR}$ spectrum is shown in Figure 3.5

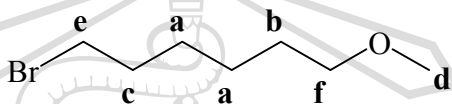


Table 3.7 $^1\text{H-NMR}$ data of 1-bromo-6-methoxyhexane

^1H position	Chemical shift (ppm)	Calculated chemical shift (ppm)
a	1.35-1.48	1.29
b	1.53-1.61	1.46
c	1.81-1.91	1.79
d-f	3.32-3.43	3.24, 3.30, 3.37

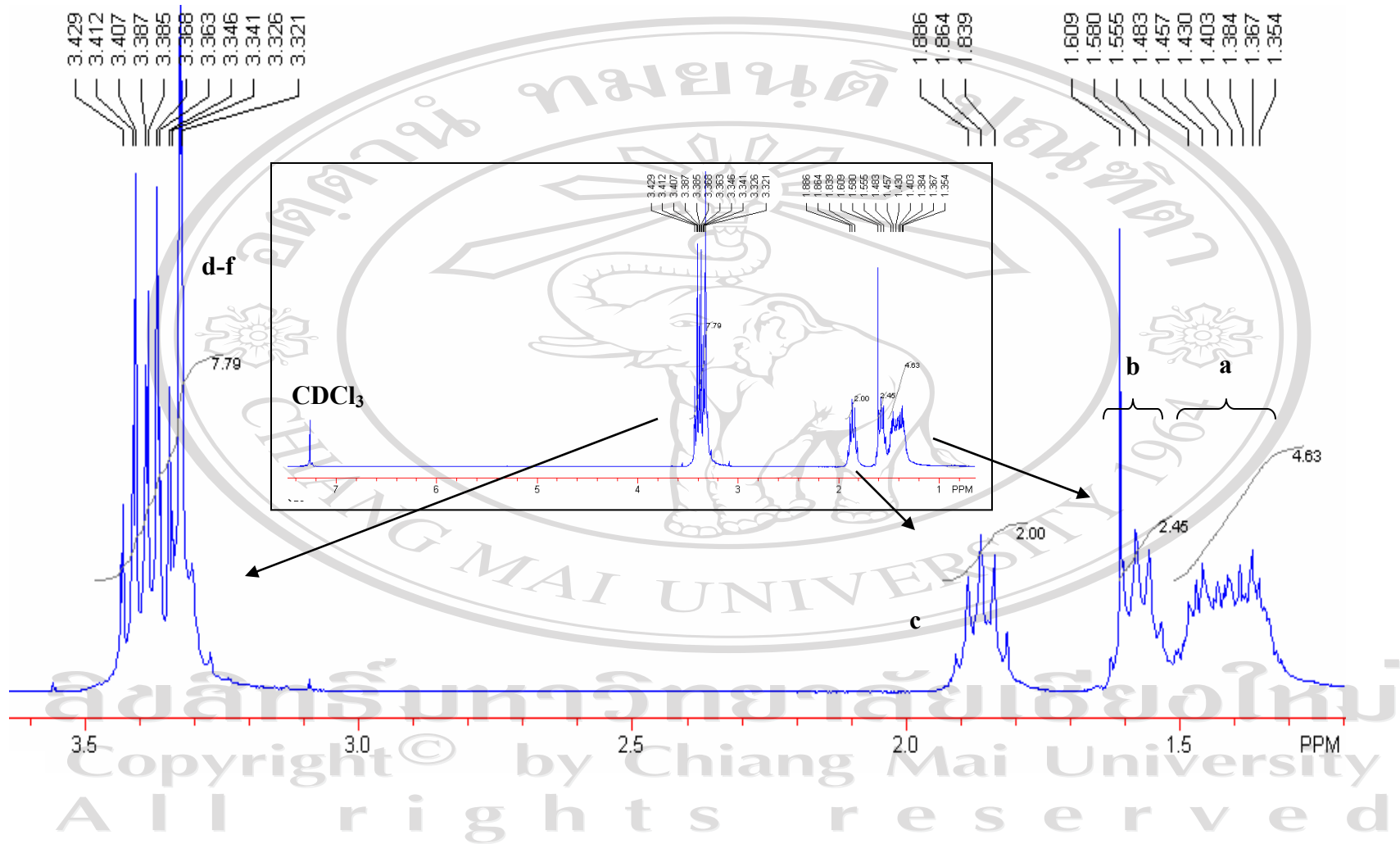


Figure 3.5 $^1\text{H-NMR}$ spectrum of 1-bromo-6-methoxyhexane in CDCl_3

3.4.2 Characterization of 2-(6-methoxyhexyl)thiophene

The $^1\text{H-NMR}$ data of 2-(6-methoxyhexyl)thiophene is shown in Table 3.8 and the $^1\text{H-NMR}$ spectrum is shown in Figure 3.6.

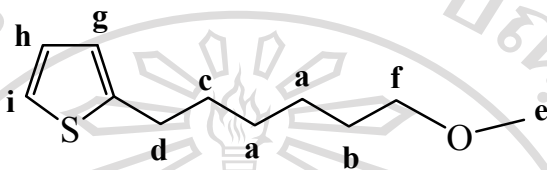


Table 3.8 $^1\text{H-NMR}$ data of 2-(6-methoxyhexyl)thiophene

^1H position	Chemical shift (ppm)	Calculated chemical shift (ppm)
a	1.36-1.57	1.29
b,c	1.60-1.71	1.46, 1.62
d	2.8-2.85	2.55
e,f	3.30-3.39	3.24, 3.37
g	6.77-6.78	6.60
h	6.90-6.93	6.72
i	7.09-7.11	6.91

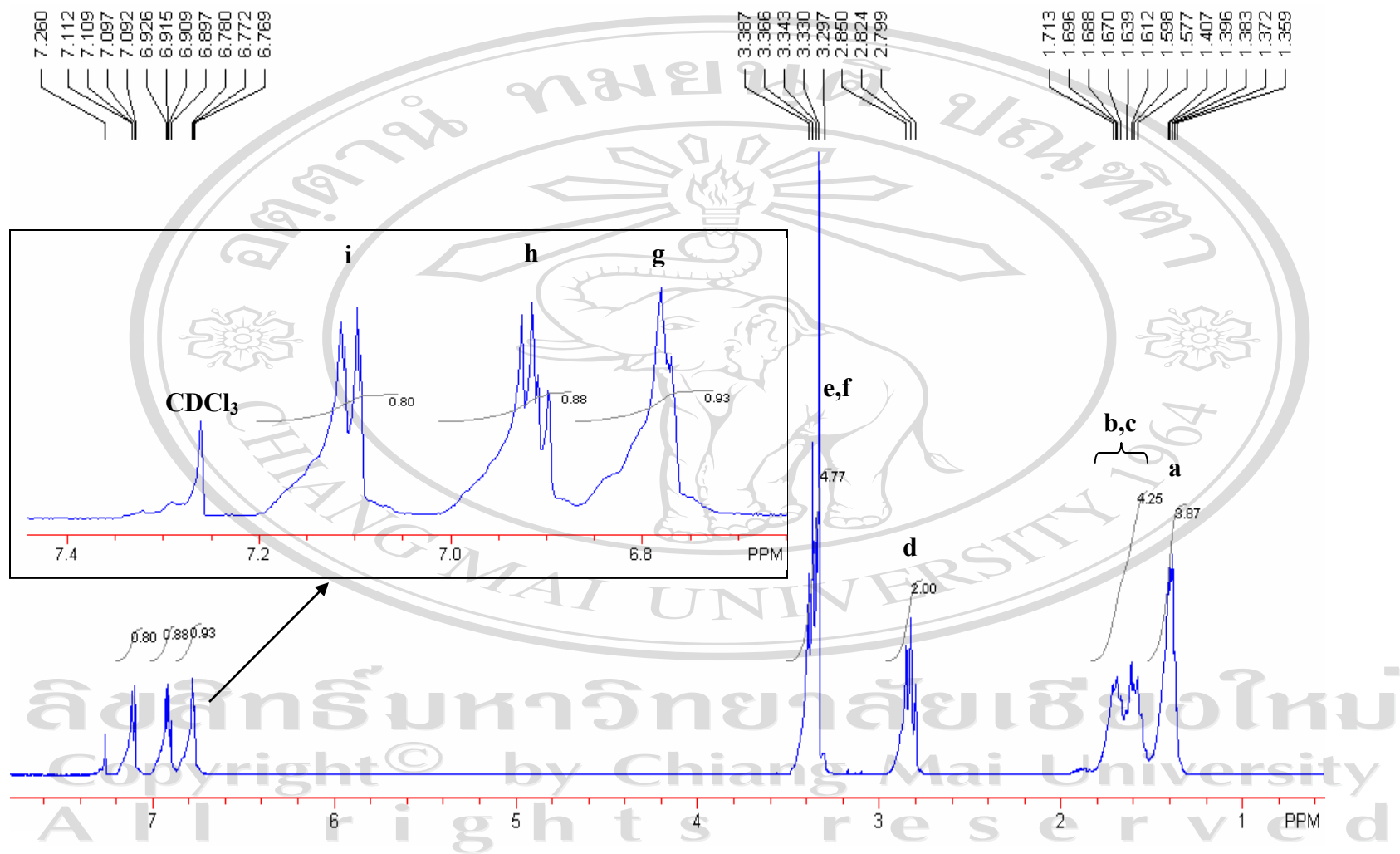


Figure 3.6 $^1\text{H-NMR}$ spectrum of 2-(6-methoxyhexyl)thiophene in CDCl_3

3.4.3 Characterization of tributyl(5-(6-methoxyhexyl)thiophen-2-yl)stannane

The $^1\text{H-NMR}$ data of tributyl(5-(6-methoxyhexyl)thiophen-2-yl)stannane is shown in Table 3.9 and the $^1\text{H-NMR}$ spectrum is shown in Figure 3.7.

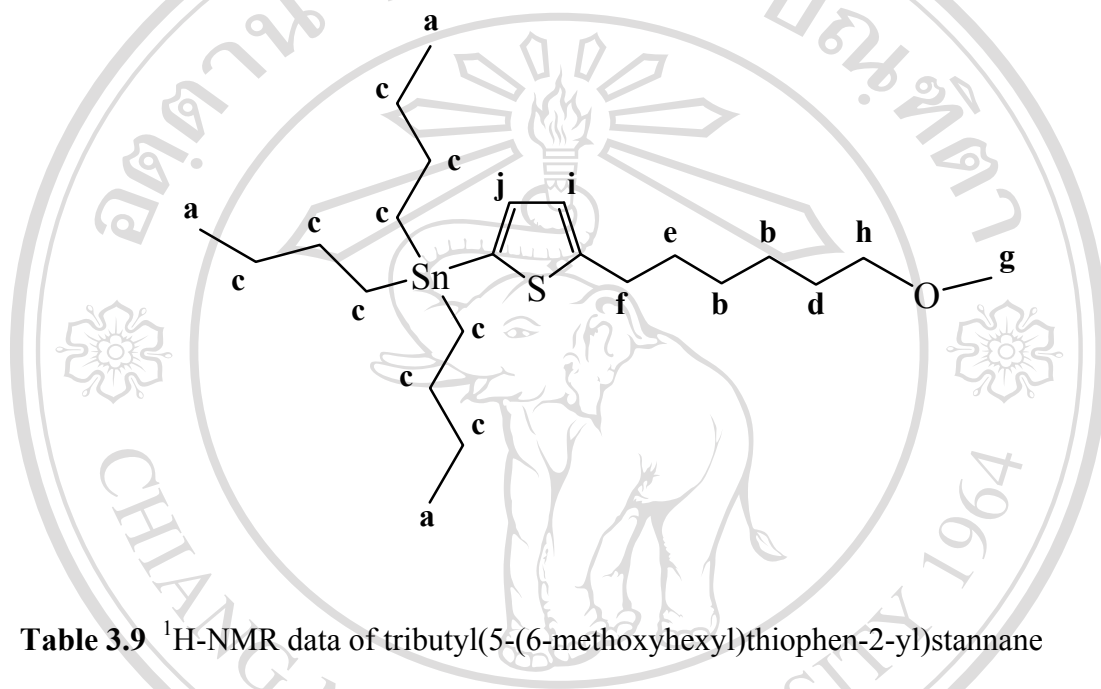


Table 3.9 $^1\text{H-NMR}$ data of tributyl(5-(6-methoxyhexyl)thiophen-2-yl)stannane

^1H position	Chemical shift (ppm)	Calculated chemical shift (ppm)
a	0.86-0.93	0.96
b,d,e	1.52-1.64	1.29, 1.46, 1.62
c	1.04-1.13 and 1.27-1.39	1.3
f	2.83-2.88	2.55
g,h	3.32, 3.34-3.38	3.24, 3.37
i	6.89-6.91	6.6
j	6.97-6.98	6.7

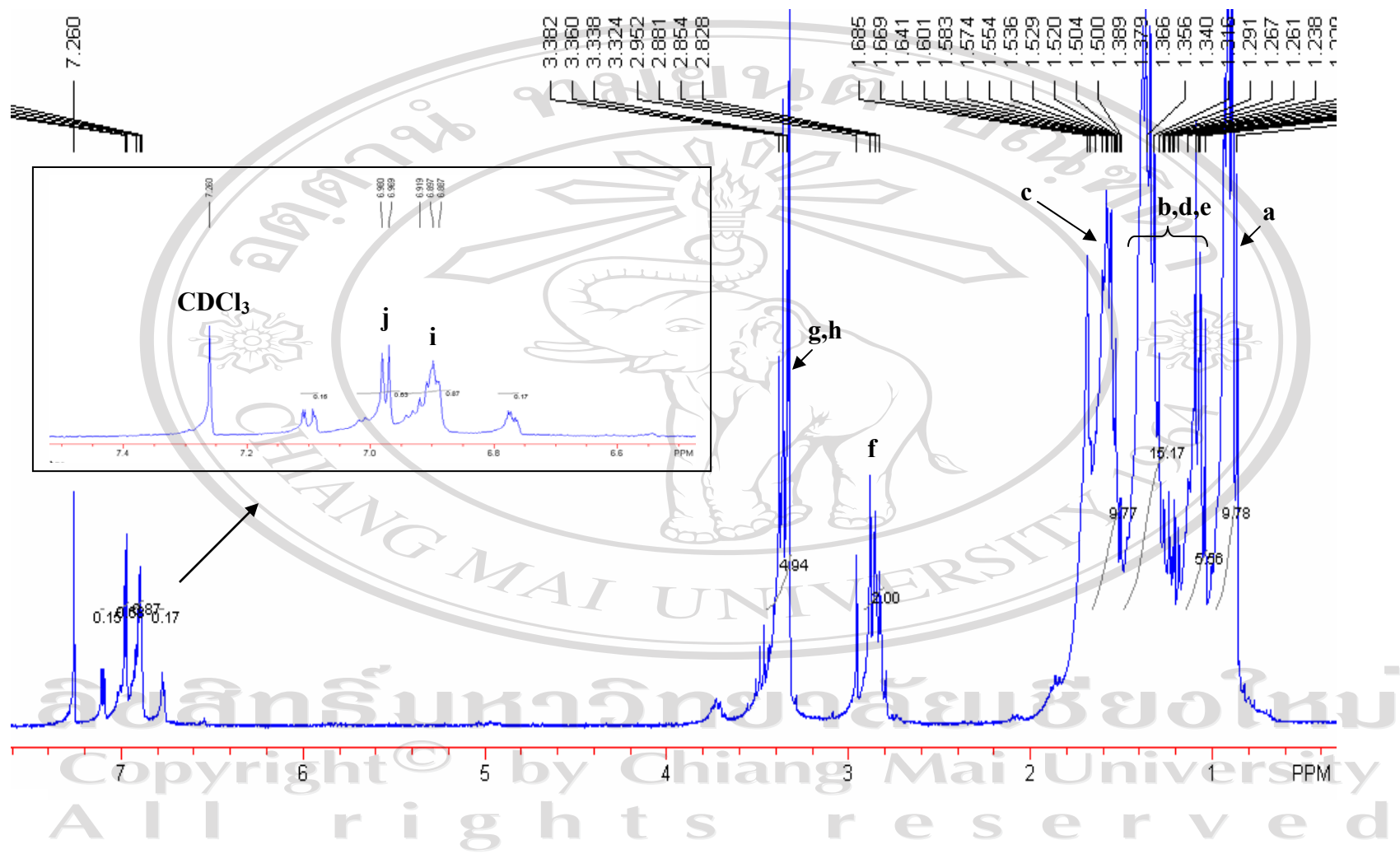


Figure 3.7 ¹H-NMR spectrum of tributyl(5-(6-methoxyhexyl)thiophen-2-yl)stannane in CDCl₃

3.4.4 Characterization of 2,3-bis(5-(6-methoxyhexyl)thiophen-2-yl)thiophene

The $^1\text{H-NMR}$ data of 2,3-bis(5-(6-methoxyhexyl)thiophen-2-yl)thiophene is shown in Table 3.10 and the $^1\text{H-NMR}$ spectrum is shown in Figure 3.8.

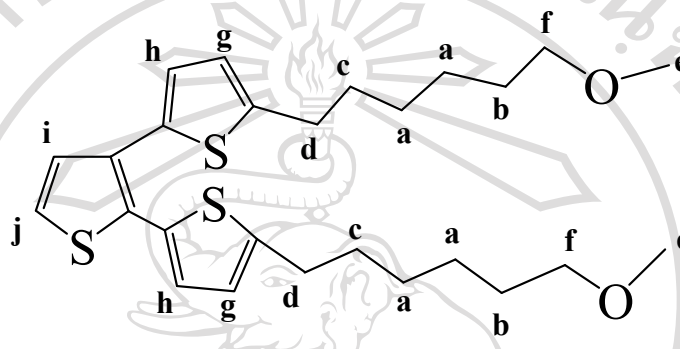


Table 3.10 $^1\text{H-NMR}$ data of 2,3-bis(5-(6-methoxyhexyl)thiophen-2-yl)thiophene

^1H position	Chemical shift (ppm)	Calculated chemical shift (ppm)
a	1.38-1.39	1.29
b,c	1.57-1.66	1.46, 1.62
d	2.75-2.80	2.55
e,f	3.33-3.40	3.24, 3.37
g	6.64-6.65 and 6.85-6.86	6.6
h	6.67-6.68 and 6.92-6.93	6.7
i	7.10-7.12	7.0
j	7.20-7.21	7.2

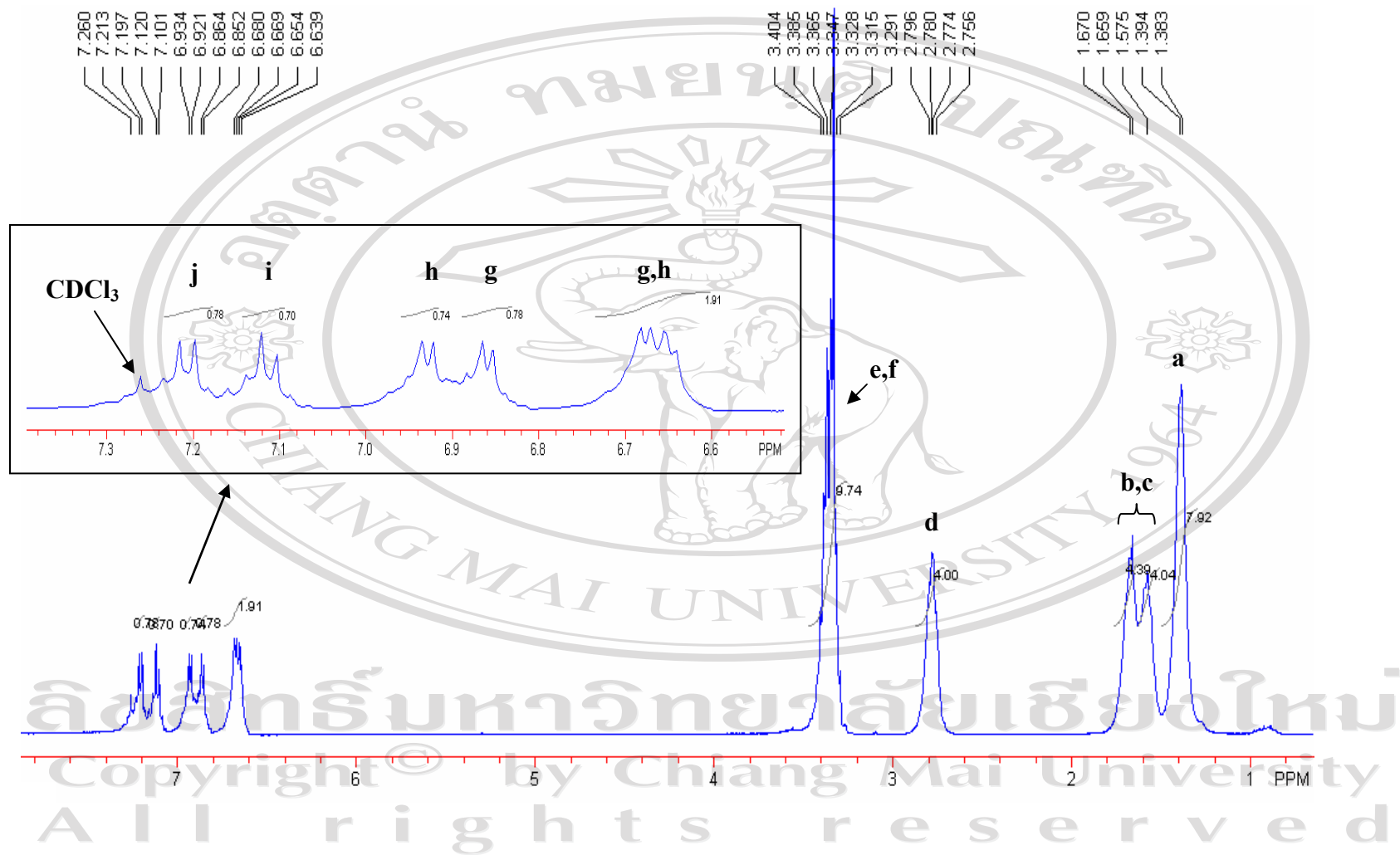


Figure 3.8 ¹H-NMR spectrum of 2,3-bis(5-(6-methoxyhexyl)thiophen-2-yl)thiophene in CDCl₃

The ^{13}C -NMR data of 2,3-bis(5-(6-methoxyhexyl)thiophen-2-yl)thiophene is shown in Table 3.11 and the ^{13}C -NMR spectrum is shown in Figure 3.9.

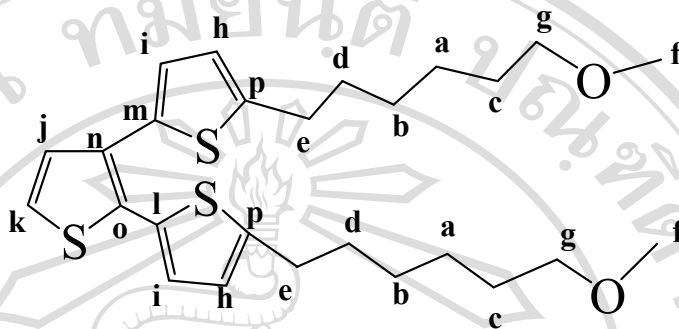


Table 3.11 ^{13}C -NMR data of 2,3-bis(5-(6-methoxyhexyl)thiophen-2-yl)thiophene

^{13}C position	Chemical shift (ppm)	Calculated chemical shift (ppm)
a	25.86	26.0
b	28.9	29.3
c	29.5	29.8
d	30.0-30.03	32.0
e	31.45-31.5	43.1
f	58.56	59.3
g	72.80	74.6
h	123.99-124.18	125.9
i	125.91	126.8
j	127.61	127.61

Table 3.11 (continued)

¹³ C position	Chemical shift (ppm)	Calculated chemical shift (ppm)
k	129.60	128.1
l	131.28	134.2
m	132.04-132.31	135.5
n	134.99	138.4
o	145.78	138.8
p	147.28	143

ลิขสิทธิ์มหาวิทยาลัยเชียงใหม่
 Copyright© by Chiang Mai University
 All rights reserved

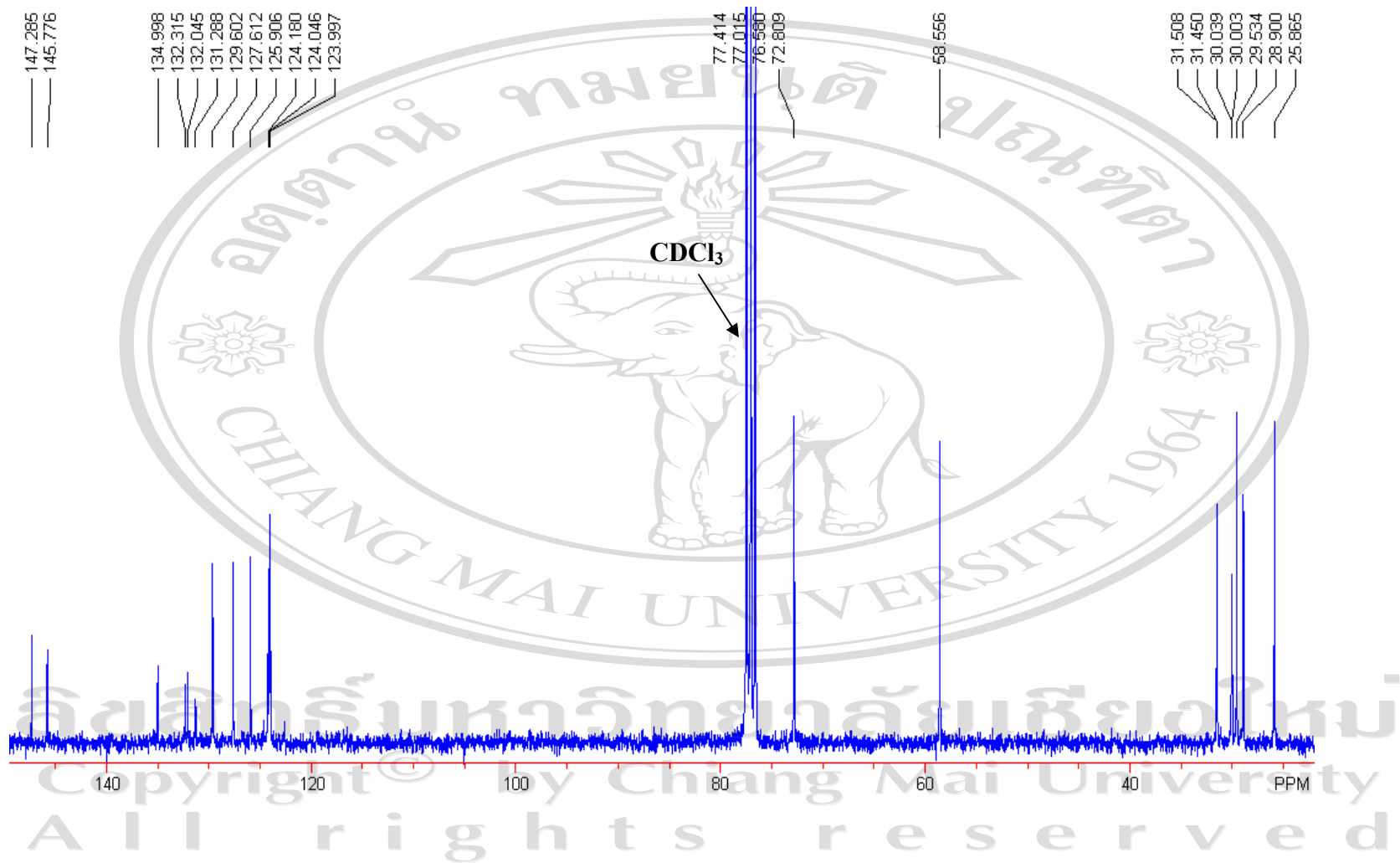


Figure 3.9 ^{13}C -NMR spectrum of 2,3-bis(5-(6-methoxyhexyl)thiophen-2-yl)thiophene in CDCl_3

3.4.5 Characterization of 5-(4,5-bis(5-(6-methoxyhexyl)thiophen-2-yl)thiophen-2-yl)-2,3-bis(5-(6-methoxyhexyl)thiophen-2-yl)thiophene

The $^1\text{H-NMR}$ data of 5-(4,5-bis(5-(6-methoxyhexyl)thiophen-2-yl)thiophen-2-yl)-2,3-bis(5-(6-methoxyhexyl)thiophen-2-yl)thiophene is shown in Table 3.12 and the $^1\text{H-NMR}$ spectrum is shown in Figure 3.10.

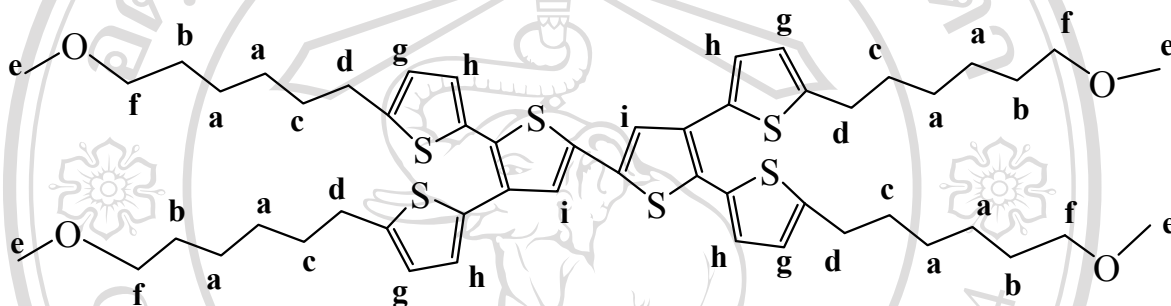


Table 3.12 $^1\text{H-NMR}$ data of 5-(4,5-bis(5-(6-methoxyhexyl)thiophen-2-yl)thiophen-2-yl)-2,3-bis(5-(6-methoxyhexyl)thiophen-2-yl)thiophene

^1H position	Chemical shift (ppm)	Calculated chemical shift (ppm)
a	1.38-1.39	1.29
b,c	1.57-1.67	1.46, 1.62
d	2.75-2.82	2.55
e,f	3.32-3.39	3.24, 3.37
g	6.66-6.68	6.6
h	6.89-6.90 and 6.94-6.96	6.7
i	7.159	7.0

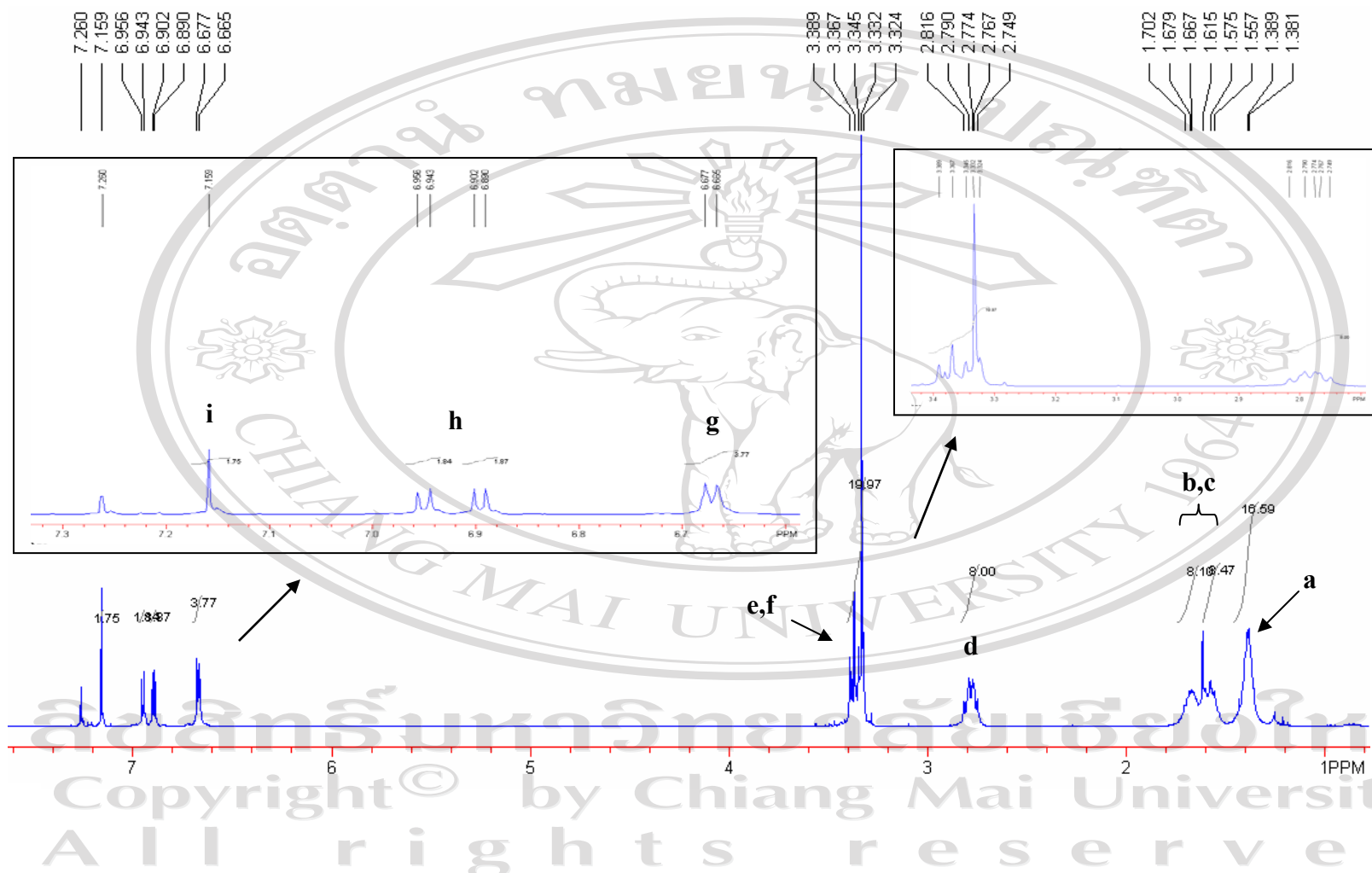


Figure 3.10 ¹H-NMR spectrum of 5-(4,5-bis(5-(6-methoxyhexyl)thiophen-2-yl)thiophen-2-yl)-2,3-bis(5-(6-methoxy

hexyl)thiophen-2-yl)thiophene in CDCl₃

The ^{13}C -NMR data of 5-(4,5-bis(5-(6-methoxyhexyl)thiophen-2-yl)thiophen-2-yl)-2,3-bis(5-(6-methoxyhexyl)thiophen-2-yl)thiophene is shown in Table 3.13 and the ^{13}C -NMR spectrum is shown in Figure 3.11.

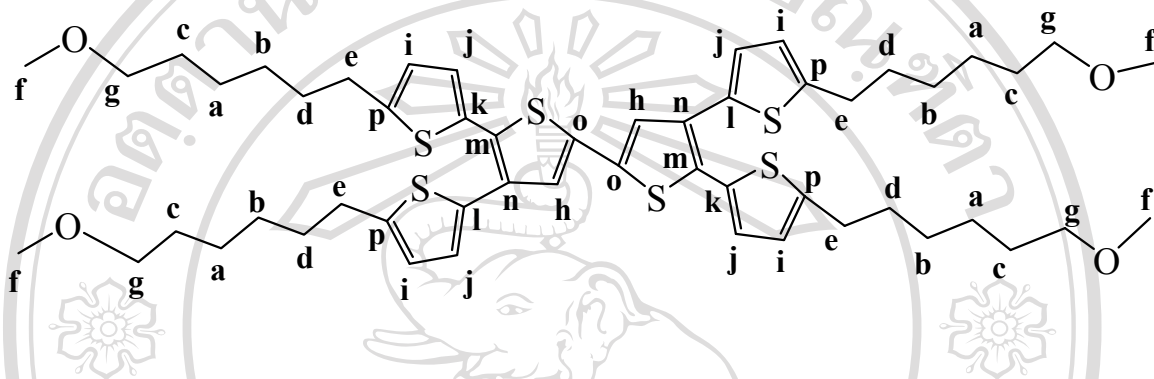


Table 3.13 ^{13}C -NMR data of 5-(4,5-bis(5-(6-methoxyhexyl)thiophen-2-yl)thiophen-2-yl)-2,3-bis(5-(6-methoxyhexyl)thiophen-2-yl)thiophene

^{13}C position	Chemical shift (ppm)	Calculated chemical shift (ppm)
a	25.85	26.0
b	28.88	29.3
c	29.53	29.8
d	30.02-30.06	32.0
e	31.44-31.52	43.1
f	58.55	59.3
g	72.78	74.6

Table 3.13 (continued)

¹³ C position	Chemical shift (ppm)	Calculated chemical shift (ppm)
h	124.11-124.26	121.3
i	126.29-126.40	125.9
j	127.41	126.8
k	130.75	134.2
l	132.05	135.5
m	132.28	138.5
n	134.36-134.38	139.2
o	147.40	139.3
p	146.17	143

ลิขสิทธิ์มหาวิทยาลัยเชียงใหม่
 Copyright© by Chiang Mai University
 All rights reserved

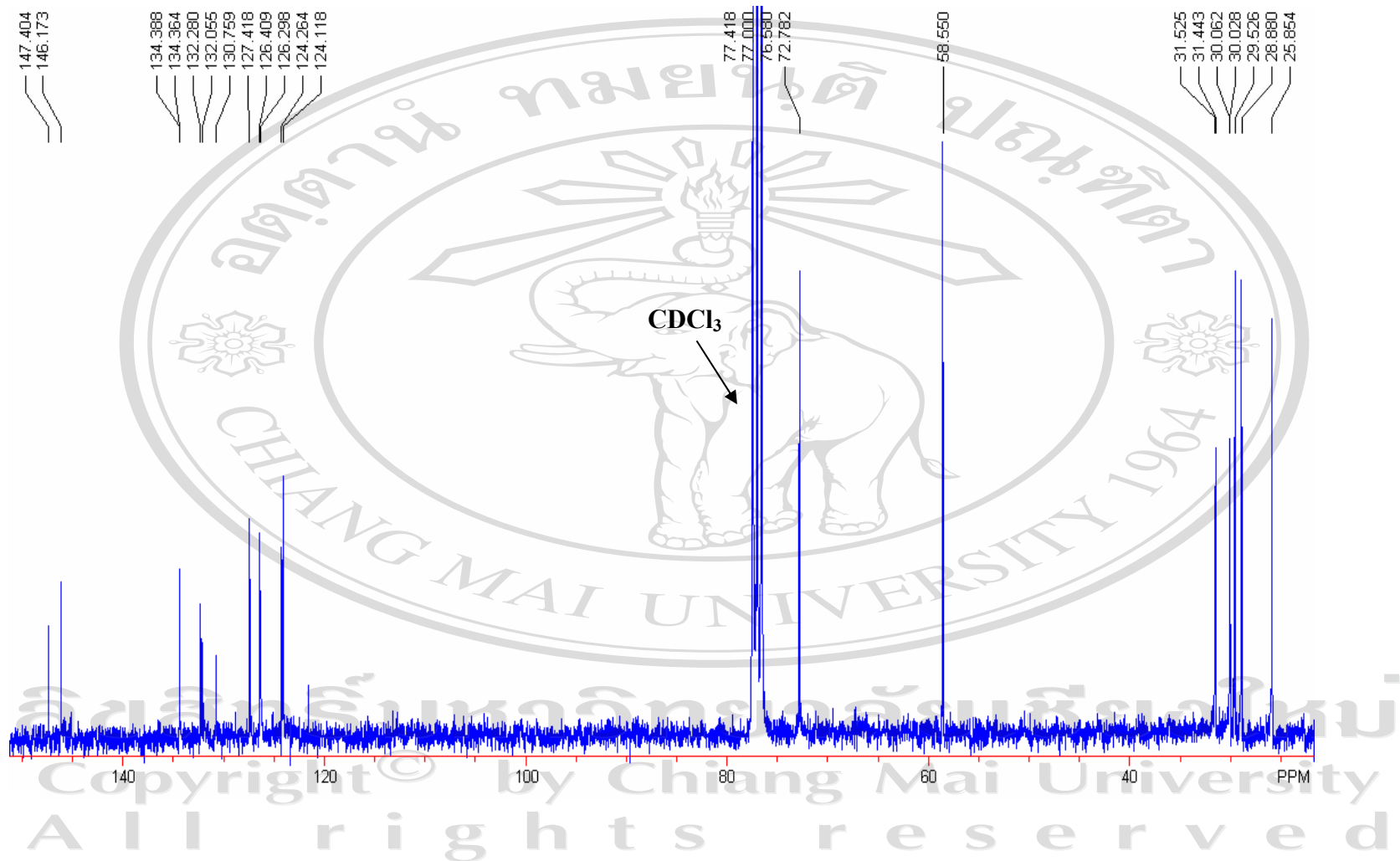


Figure 3.11 ^{13}C -NMR spectrum of 5-(4,5-bis(5-(6-methoxyhexyl)thiophen-2-yl)thiophen-2-yl)-2,3-bis(5-(6-methoxyhexyl)thiophen-2-yl)thiophene in CDCl_3

3.4.6 Characterization of 5-(4,5-bis(5-(6-bromohexyl)thiophen-2-yl)thiophen-2-yl)-2,3-bis(5-(6-bromohexyl)thiophen-2-yl)thiophene

The $^1\text{H-NMR}$ data of 5-(4,5-bis(5-(6-bromohexyl)thiophen-2-yl)thiophen-2-yl)-2,3-bis(5-(6-bromohexyl)thiophen-2-yl)thiophene is shown in Table 3.14 and the $^1\text{H-NMR}$ spectrum is shown in Figure 3.12.

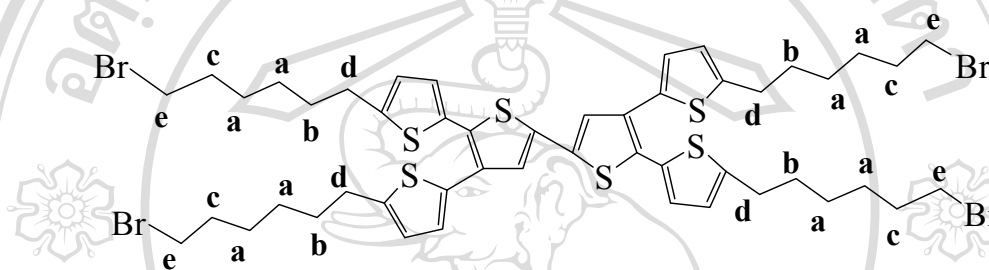


Table 3.14 $^1\text{H-NMR}$ data of 5-(4,5-bis(5-(6-bromohexyl)thiophen-2-yl)thiophen-2-yl)-2,3-bis(5-(6-bromohexyl)thiophen-2-yl)thiophene

^1H position	Chemical shift (ppm)	Calculated chemical shift (ppm)
a	1.40-1.56	1.29
b	1.66-1.69	1.62
c	1.84-1.89	1.79
d	2.76-2.83	2.55
e	3.39-3.43	3.30
f	6.67-6.69	6.6
g	6.89-6.91 and 6.95-6.96	6.7
h	7.16	7.0

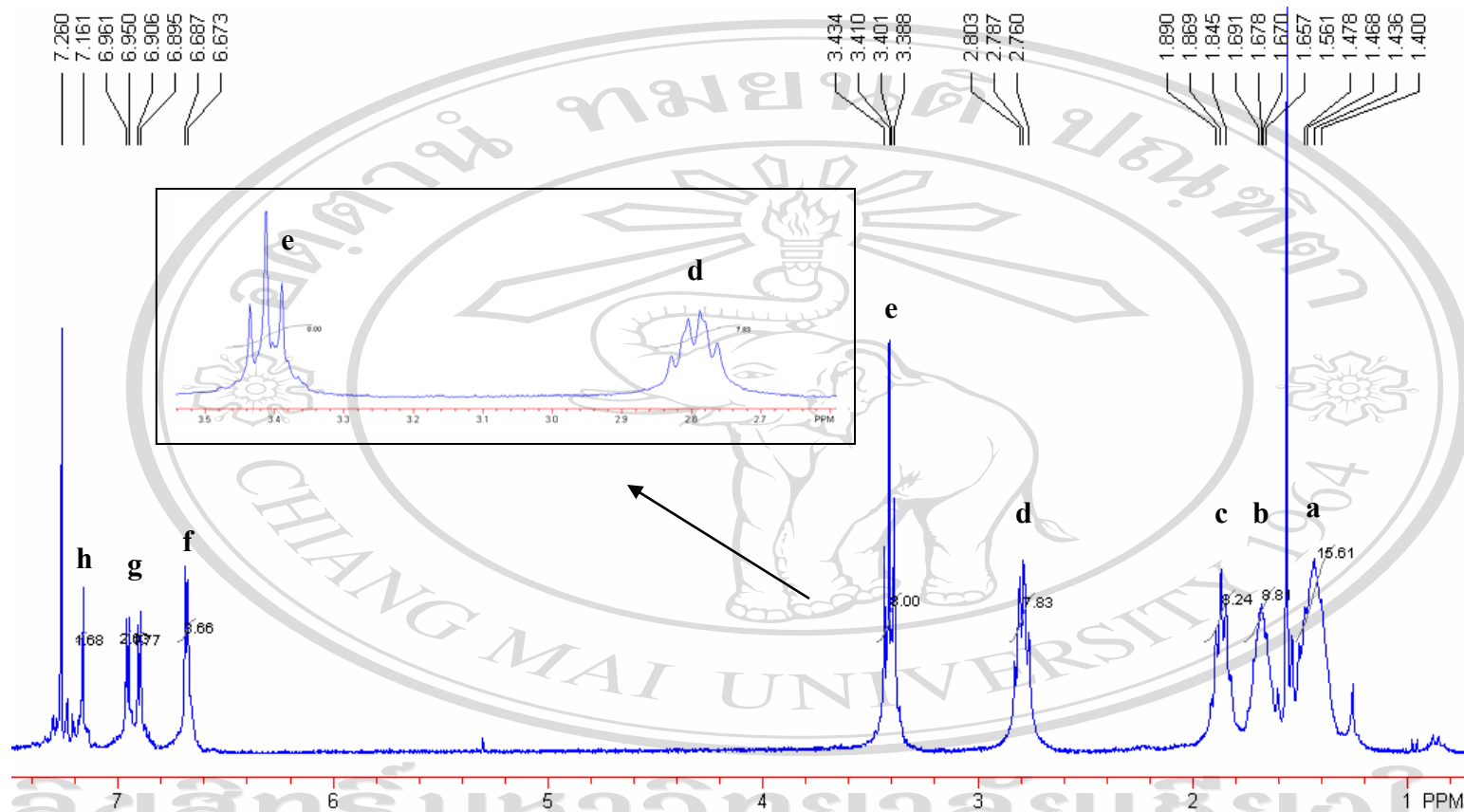


Figure 3.12 $^1\text{H-NMR}$ spectrum of 5-(4,5-bis(5-(6-bromohexyl)thiophen-2-yl) thiophen-2-yl)-2,3-bis(5-(6-bromo

hexyl)thiophen-2-yl)thiophene in CDCl_3

The ^{13}C -NMR data of 5-(4,5-bis(5-(6-bromohexyl)thiophen-2-yl)thiophen-2-yl)-2,3-bis(5-(6-bromohexyl)thiophen-2-yl)thiophene is shown in Table 3.15 and the ^{13}C -NMR spectrum is shown in Figure 3.13.

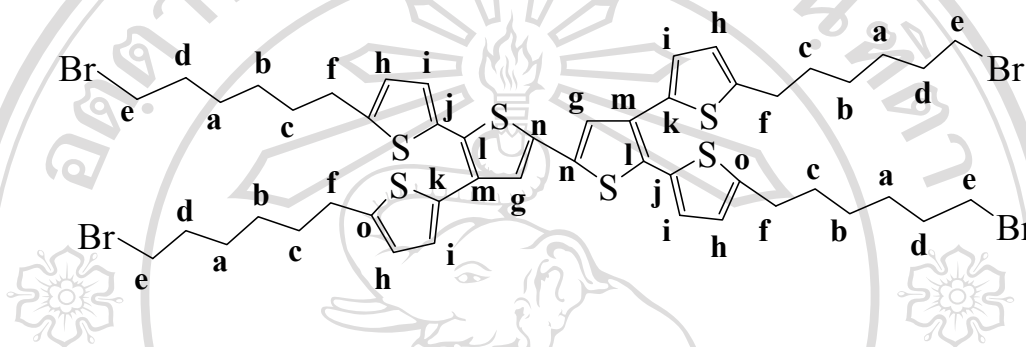


Table 3.15 ^{13}C -NMR data of 5-(4,5-bis(5-(6-bromohexyl)thiophen-2-yl) thiophen-2-yl)-2,3-bis(5-(6-bromohexyl)thiophen-2-yl)thiophene

^{13}C position	Chemical shift (ppm)	Calculated chemical shift (ppm)
a	27.84	28.1
b	28.12	28.3
c	29.97-30.00	32.0
d	31.28-31.36	32.7
e	32.65	33.7
f	33.92	43.1
g	124.23-124.39	121.3

Table 3.15 (continued)

¹³ C position	Chemical shift (ppm)	Calculated chemical shift (ppm)
h	126.31-126.46	125.9
i	127.48	126.8
j	130.78	134.2
k	132.14	135.5
l	132.3	138.5
m	134.39-134.47	139.2
n	145.93	139.3
o	147.17	143

ลิขสิทธิ์มหาวิทยาลัยเชียงใหม่
 Copyright© by Chiang Mai University
 All rights reserved

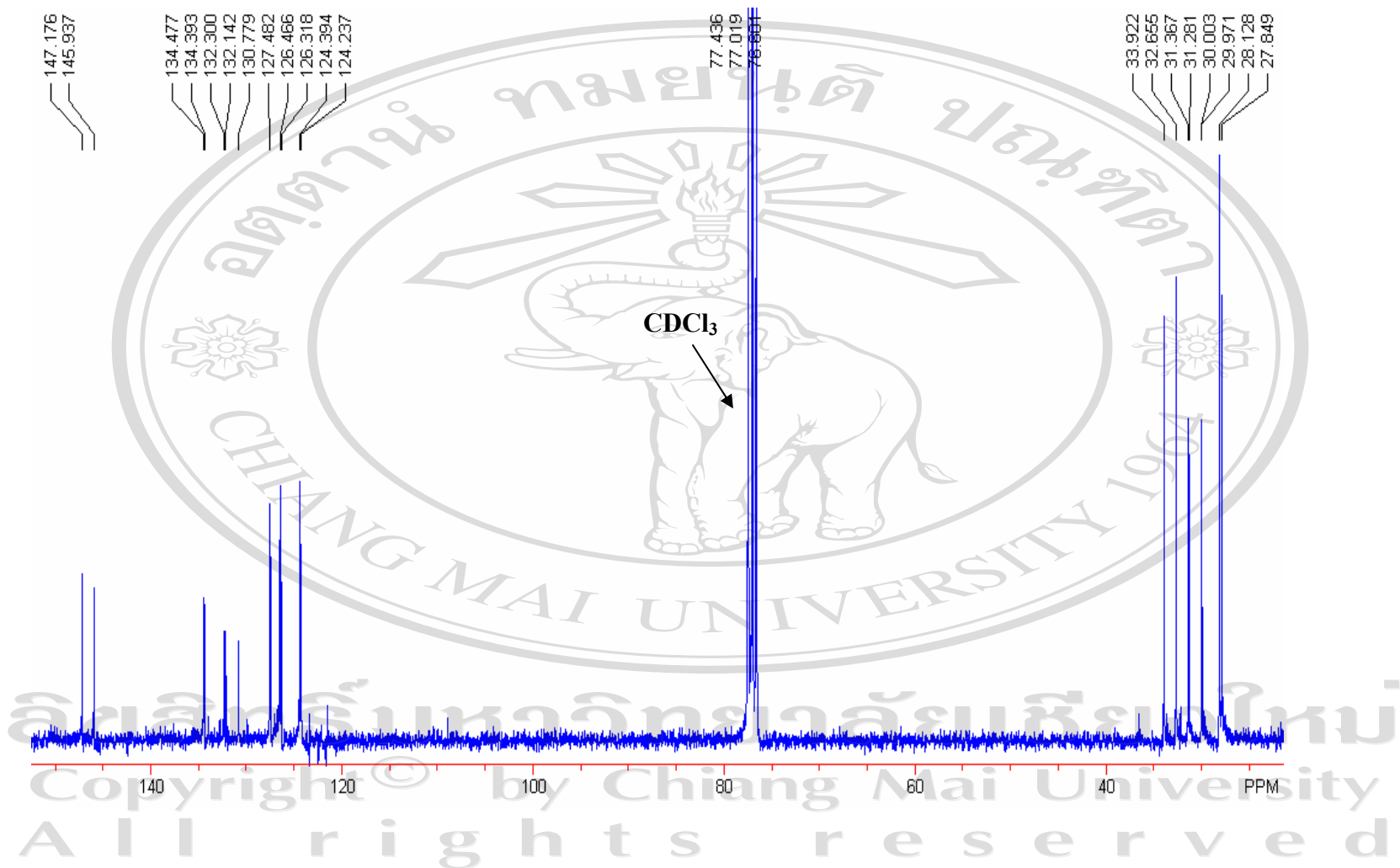


Figure 3.13 ^{13}C -NMR spectrum of 5-(4,5-bis(5-(6-bromohexyl)thiophen-2-yl)thiophen-2-yl)-2,3-bis(5-(6-bromo hexyl)thiophen-2-yl)thiophene in CDCl_3

3.4.7 Characterization of 6TND

The $^1\text{H-NMR}$ data of 6TND is shown in Table 3.16 and the $^1\text{H-NMR}$ spectrum is shown in Figure 3.14.

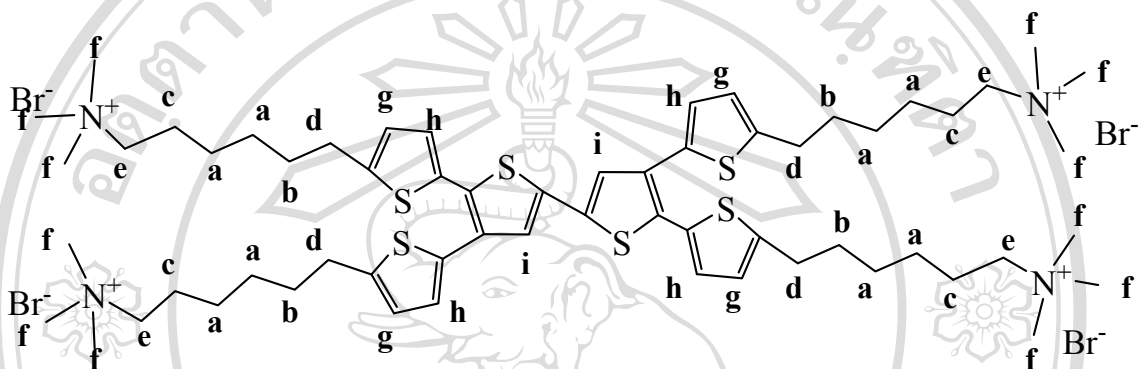


Table 3.16 $^1\text{H-NMR}$ data of 6TND

^1H position	Chemical shift (ppm)	Calculated chemical shift (ppm)
a	1.28-1.36	1.29
b,c	1.62	1.62, 1.73
d	2.73-2.80	2.55
e	3.23-3.3	3.24
f	3.37-3.49	3.30
g	6.81-6.86	6.6
h	7.05-7.09	6.7
i	7.518	7.0

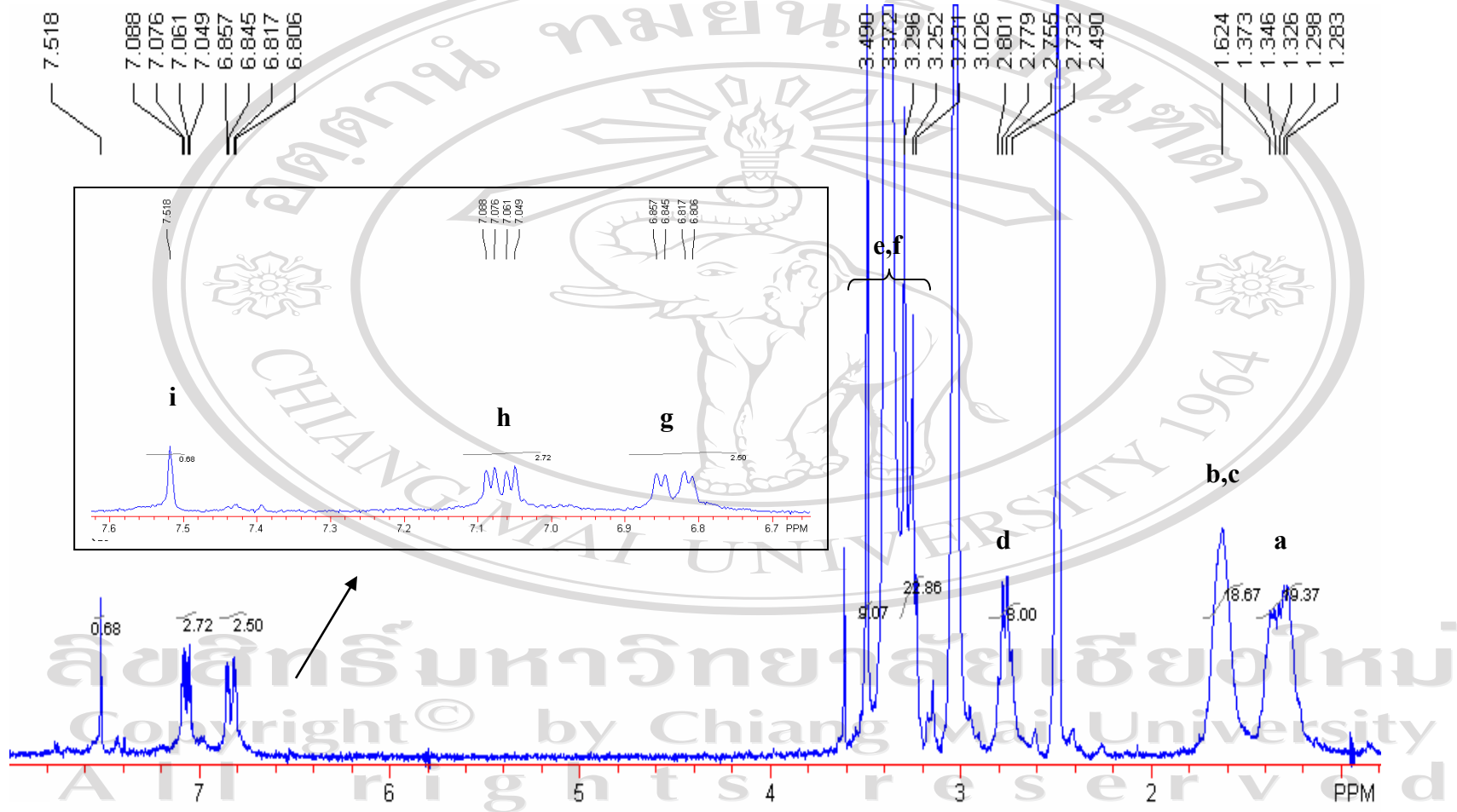


Figure 3.14 $^1\text{H-NMR}$ spectrum of 6TND in deuterated DMSO

The LC-MS data of 6TND using methanol as mobile phase is shown in Table 3.17 with the relative LC-MS spectrum as shown in Figure 3.15. The proposed structures of the observed species are also shown in Figure 3.16. The main m/z peaks at 267.3, 380.5 and 613.2 were attributed to 6TN^{4+} , 6TN^{3+} and 6TN^{2+} respectively. The m/z peak of 6TN^+ was not observed in LC-MS spectrum. This may be due to the 6TN molecule quickly lost the first 2 bromide ions and therefore the 6TN^+ could not be detected by the instrument.

Table 3.17 LC-MS data of 6TND showing 3 ion species calculated and observed m/z

Species	Calculated m/z	Observed m/z
6TN^{2+}	611.8 (1223.61/2)	613.2
6TN^{3+}	381.2 (1143.71/3)	380.5
6TN^{4+}	265.9 (1063.81/4)	267.3

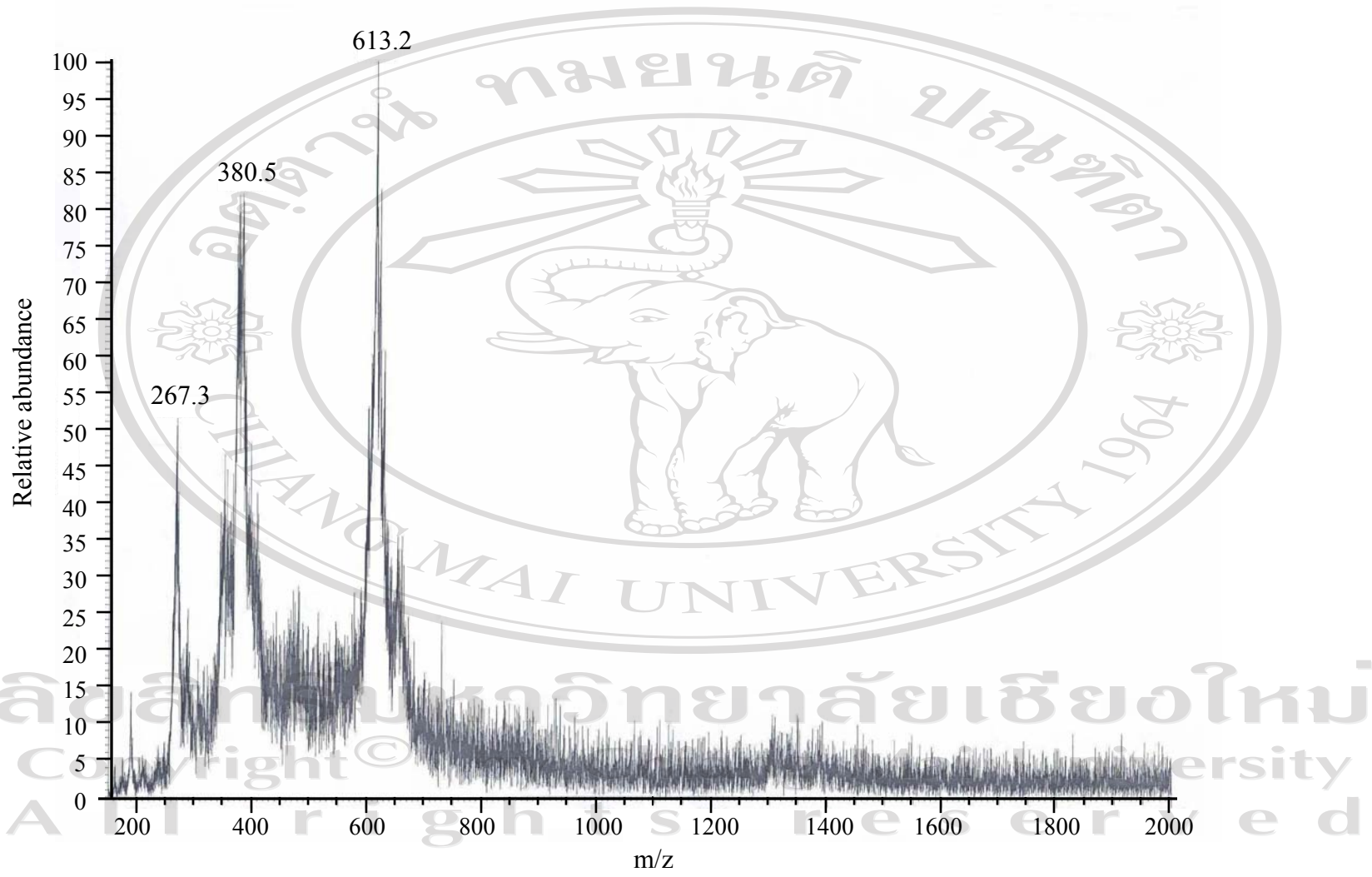


Figure 3.15 LC-MS spectrum of 6TND

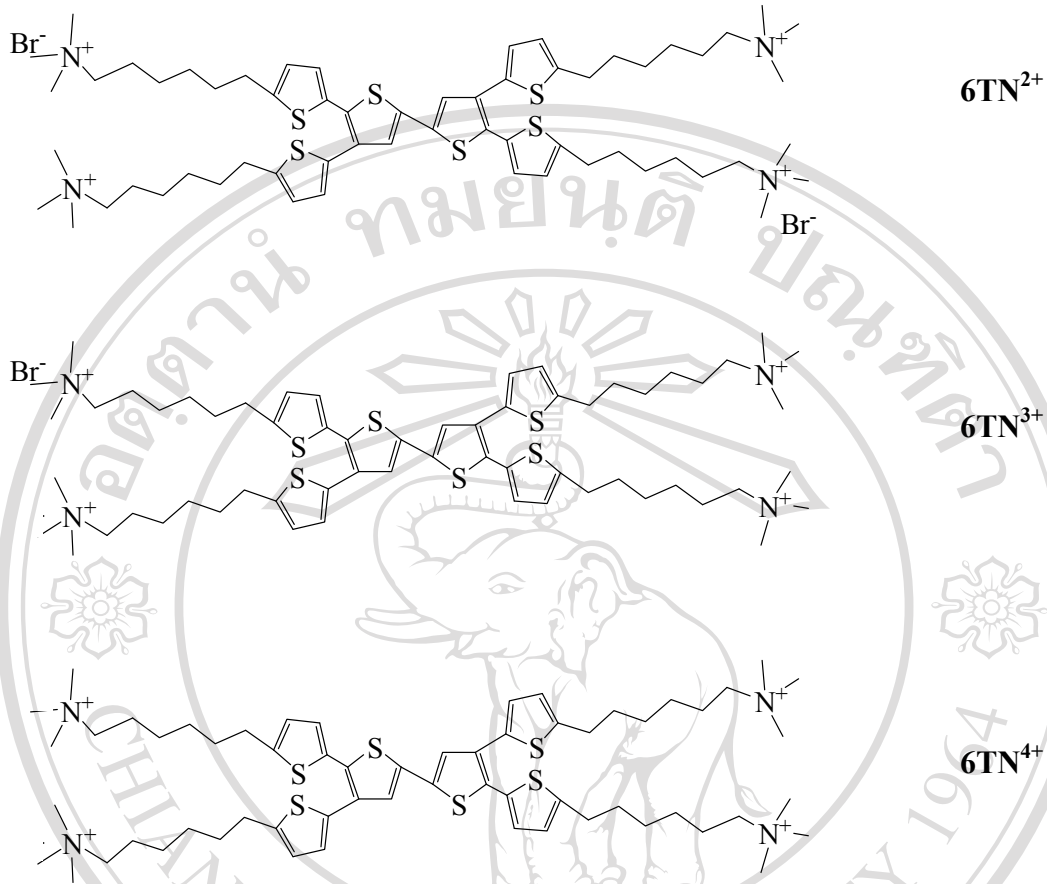


Figure 3.16 Proposed structures of the observed species from LC-MS

ลิขสิทธิ์มหาวิทยาลัยเชียงใหม่
Copyright © by Chiang Mai University
All rights reserved

3.5 Characterization of water-soluble anionic polycarbazole precursor: PCEMMA

3.5.1 Characterization of 2-(*N*-carbazolyl)ethyl methacrylate (10)

The $^1\text{H-NMR}$ data of 2-(*N*-carbazolyl)ethyl methacrylate is shown in Table 3.18 and the $^1\text{H-NMR}$ spectrum is shown in Figure 3.17.

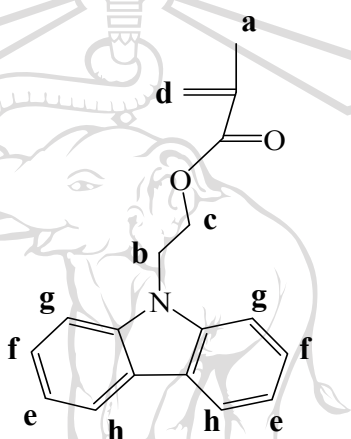


Table 3.18 $^1\text{H-NMR}$ data of 2-(*N*-carbazolyl)ethyl methacrylate

^1H position	Chemical shift (ppm)	Calculated chemical shift (ppm)
a	1.82	1.93
b	4.31-4.35	4.13
c	4.60-4.65	4.63
d	5.94	5.58, 6.15
e	7.19-7.24	7.08
f	7.36-7.48	7.12, 7.28
h	8.07-8.10	7.36

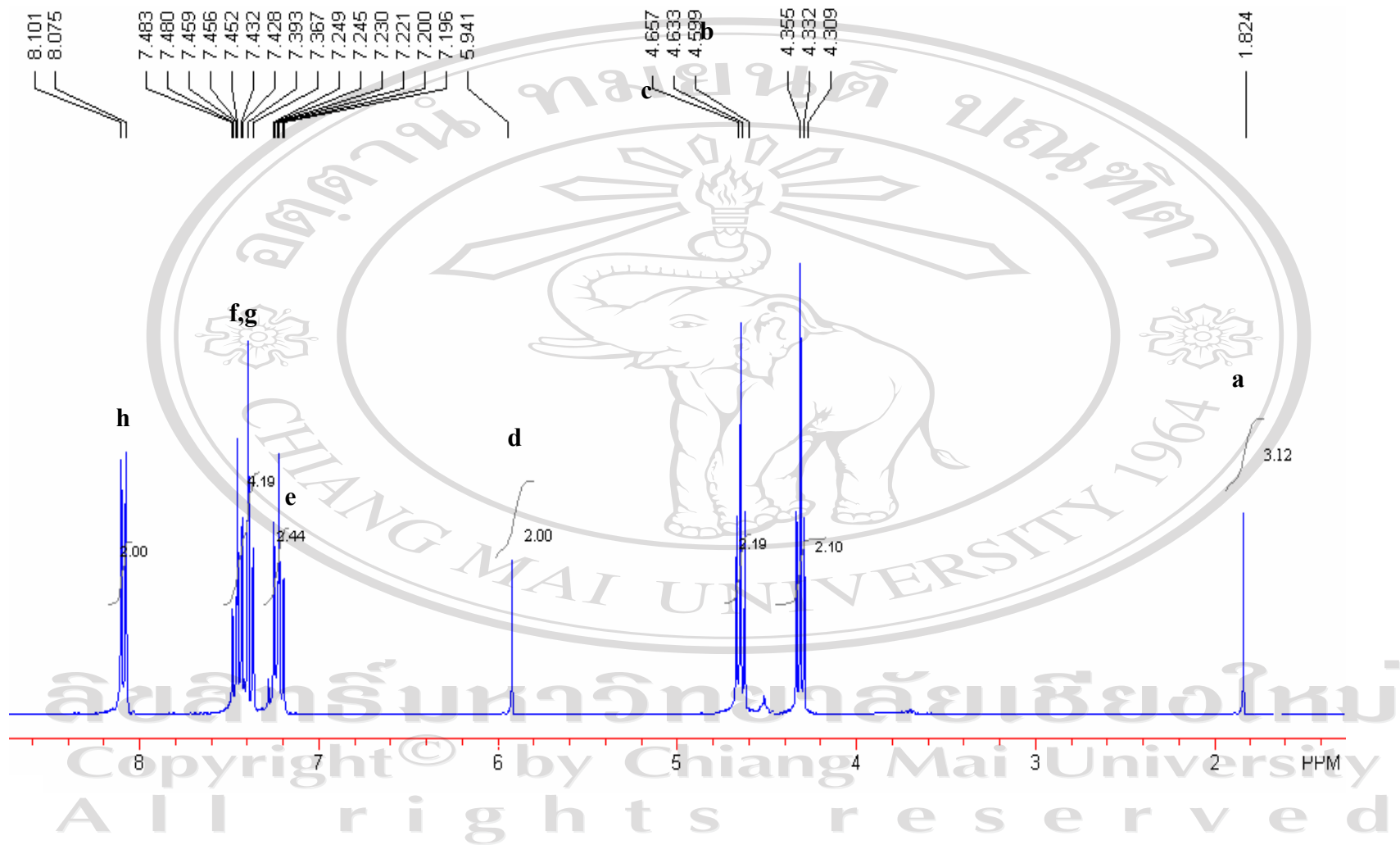


Figure 3.17 $^1\text{H-NMR}$ spectrum of 2-(*N*-carbazolyl)ethyl methacrylate in CDCl_3

3.5.2 Characterization of PCEMMA

The $^1\text{H-NMR}$ data of PCEMMA is shown in Table 3.19 and the $^1\text{H-NMR}$ spectrum is shown in Figure 3.18.

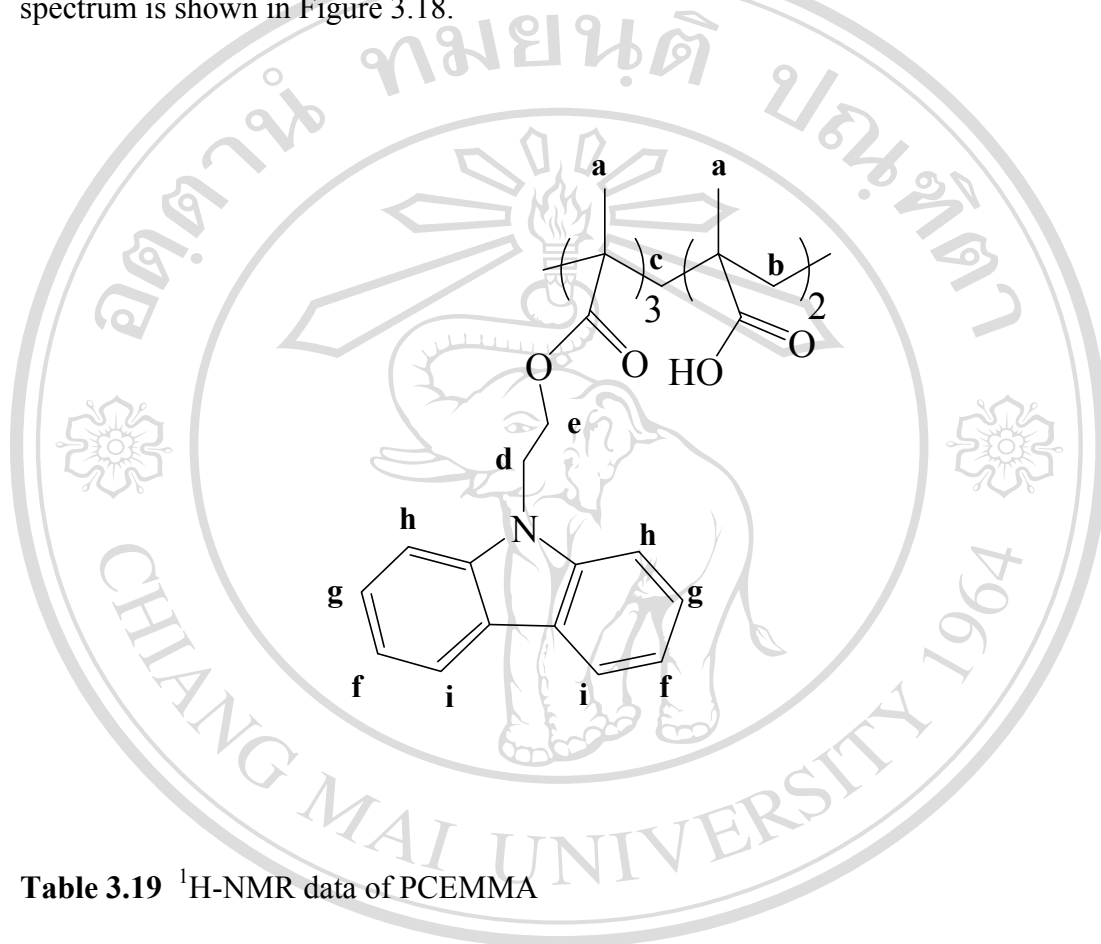
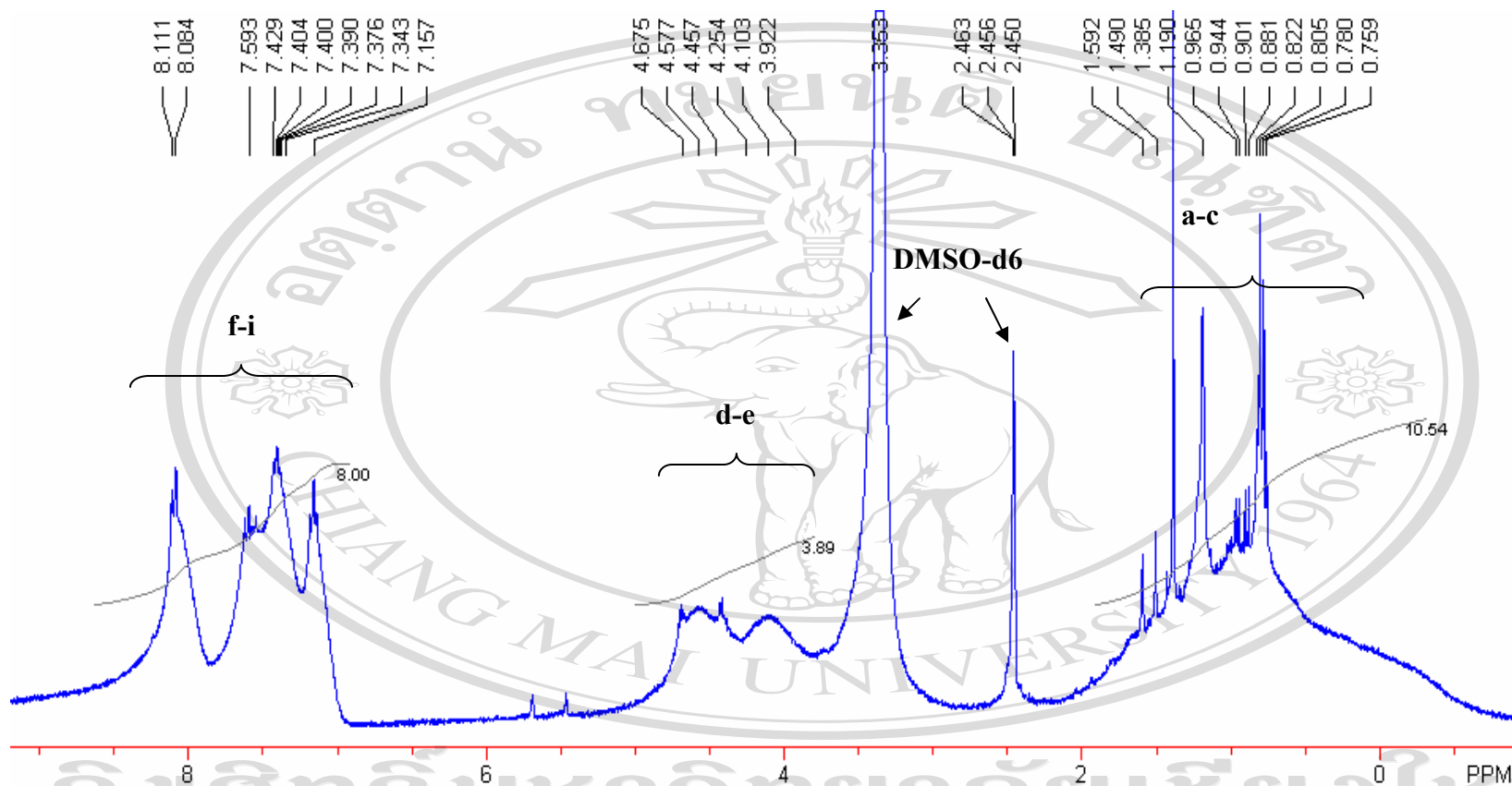


Table 3.19 $^1\text{H-NMR}$ data of PCEMMA

^1H position	Chemical shift (ppm)	Calculated chemical shift (ppm)
a,b,c	0.75-1.52	1.29, 1.52, 1.79
d,e	4.07-4.69	4.13, 4.56
f,g,h,i	7.15-7.59 and 8.08-8.11	7.08, 7.12, 7.28, 7.36



ลิขสิทธิ์มหาวิทยาลัยเชียงใหม่
 Copyright© by Chiang Mai University
 All rights reserved

Figure 3.18 $^1\text{H-NMR}$ spectrum of PCEMMA in deuterated DMSO

3.6 UV-Vis and photoluminescence spectra of 6TNL, 6TND and PCEMMA

The UV-Vis absorption spectra of 6TNL and 6TND in water and PCEMMA in water/DMSO (2/3 v/v) at pH 10 are shown in Figure 3.19. The dendrimeric sexithiophene shows spectroscopic properties that are different from the linear sexithiophene. As described before [57], there are two different linkages between each thiophene units including α,β and α,α linkages. The α,α linkage provides the best π -electron conjugation while α,β linkage may disrupt it. The absorption spectrum of 6TND showed three peaks at 385, 294, 252 nm, originating from the π - π^* transitions. The lowest energy absorption at 385 nm was almost identical to α -quaterthiophene. The absorption spectrum of 6TNL showed the strongest π - π^* transition peak at 423 nm and several shoulders or peaks at around 440, 470 and 515 nm respectively. These distinct shoulders could be due to the vibronic structure and/or Davydov interaction. As shown in the structures of 6TND and 6TNL which have both hydrophobic sexithiophene units and cationic alkyl chain arms at the ends. The positively charged quaternized amine end groups make molecules hydrophilic and water soluble. However, due to 6TND has 4 quaternized amine end groups which lead to greater solubility than 6TNL which has 2 quaternized amine end groups. Moreover, in the previous studies of Advincula group [28, 50], they observed that the shoulder peaks of 6TNL in water were originated from H-aggregation (π - π stacking) which were disappeared when added THF (up to 30%) to this aqueous solution. This phenomenon could not be observed in case of 6TND in water. The UV-Vis absorption spectra of 6TND in different ratio of water/THF were identical. This observation was also

consistent with the photoluminescence spectra, i.e., the photoluminescence could be observed for 6TND in water and was quenched in water for 6TNL. The UV-Vis spectrum of PCEMMA showed the peaks at 245, 261, 293, 332, 345 nm which were attributed from π - π^* and n - π^* transitions of carbazole unit which presented as polymer pendant side groups [22].

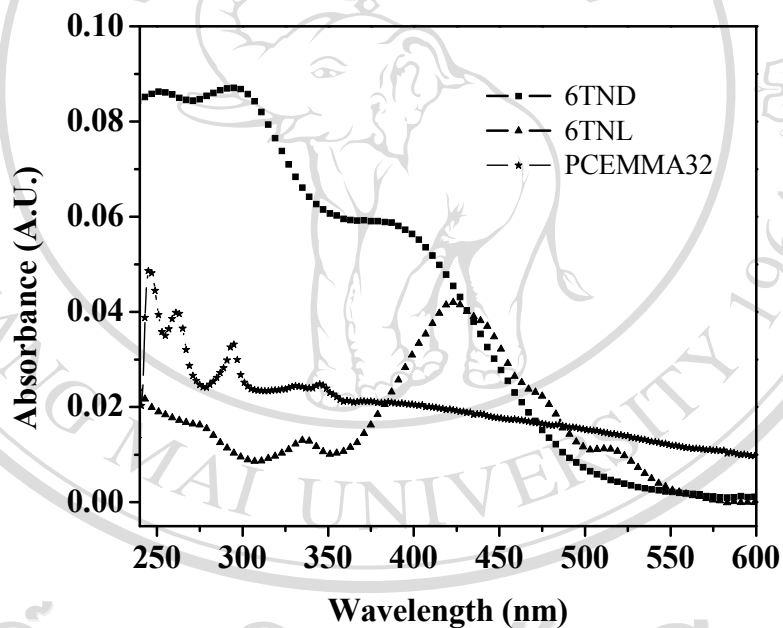


Figure 3.19 UV-Vis absorption spectra of 6TNL and 6TND in water and PCEMMA in DMSO/water (2/3 v/v) at pH 10

3.7 Layer-by-layer deposition

3.7.1 UV-Vis spectra of deposited films

The multilayer films of 6TNL and 6TND with PCEMMA on various substrates were performed by the layer-by-layer deposition technique. The deposition of layer was monitored by using UV-Vis absorption spectroscopy on quartz substrate in every 2 bi-layers. The UV-Vis absorption spectra of the films prepared from 6TNL and 6TND are shown in Figure 3.20 (a) and (b) respectively. The absorbance intensity of both 6TNL and 6TND increased linearly with increasing number of layers indicating a stepwise and regular growth process. The relationship between the peak intensity at 262 nm and the number of deposition layers in two systems is shown in Figure 3.21. As shown in UV-Vis absorption spectra of 6TNL and 6TND in solution, the absorbance intensity of 6TND system was higher than 6TNL system even though the conjugation linkage for 6TNL molecule is better than 6TND molecule. As from the well-known Beer-Lambert Law, the absorbance is directly proportional to molar absorptivity at constant concentration and path length. The compound with higher molar absorptivity is more effective at absorbing wavelength and hence the low concentration of the compound with higher molar absorptivity can be easier detected. This indicated that 6TND has higher molar absorptivity than 6TNL.

The different between UV-Vis absorption peaks of 6TND in solution and film could be observed. The red shift of the peak at 385 nm, which attributed from thiophene unit, in water solution to about 400-425 nm in film is due to the J-aggregation of 6TND in film. This result was possibly from the interaction between dendrimeric sexithiophene

and polycarbazole precursor molecule which led to rearrangement of 6TND on the surface. The different between the absorption peaks of 6TNL in solution and film could also be observed. As seen from the shoulder peaks in solution, the aggregation of 6TNL was observed due to the H-aggregation. These shoulders were disappeared in film with polycarbazole precursor molecule. This result was contradictory to the results that previously described in the Advincula group which 6TNL molecule encountered the aggregation on the films [28]. The disappearance of these vibronic structure bands after adsorption with this polycarbazole precursor layer showed that deaggregation could be occurred during the adsorption process.

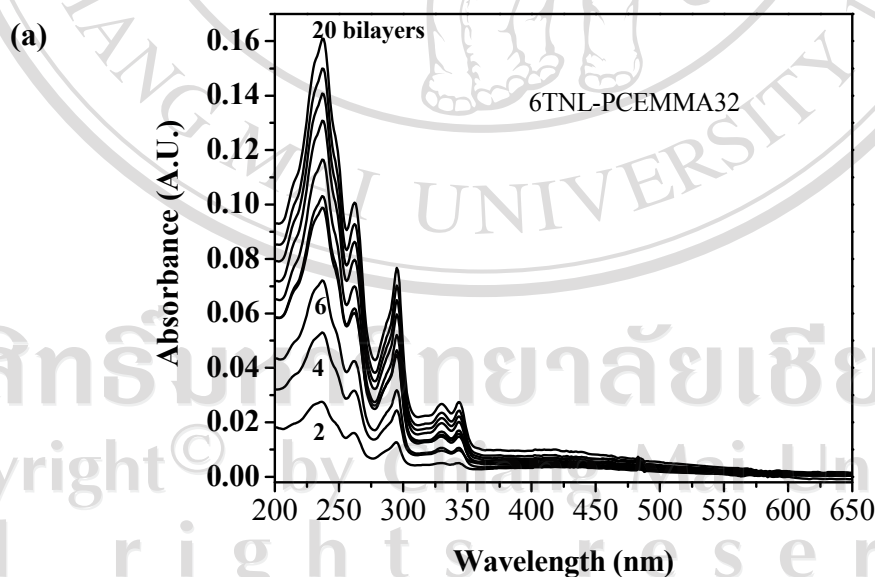


Figure 3.20 UV-Vis spectra of (a) 6TNL-PCEMMA and (b) 6TND-PCEMMA multilayer films on quartz substrate (up to 20 bi-layers)

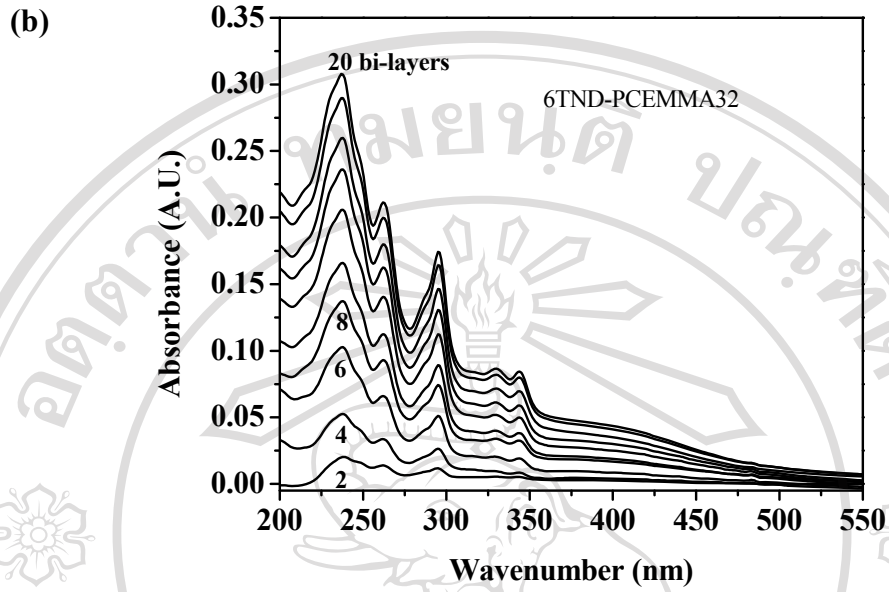


Figure 3.20 (continued)

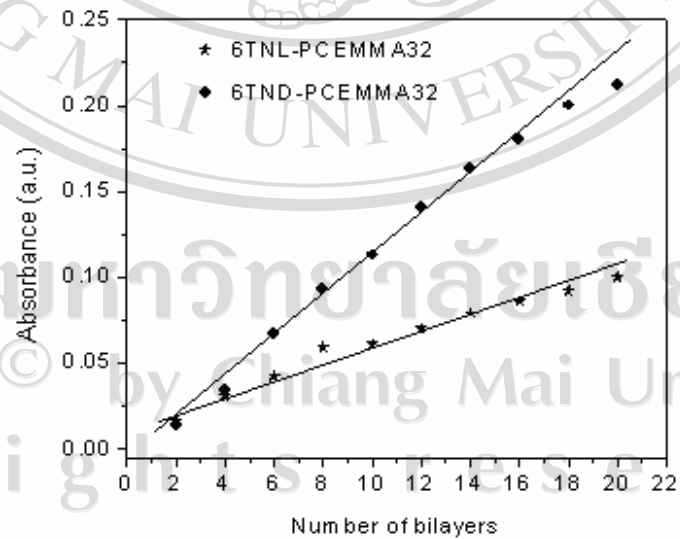


Figure 3.21 Plots of absorbance at 262 nm vs number of bi-layers in 6TNL and 6TND with PCEMMA on quartz substrate (up to 20 bi-layers)

3.7.2 *In situ* investigation of adsorption process by SPS

The kinetic of layer-by-layer adsorption for both 6TNL and 6TND system was studied by simultaneous SPS at a fixed angle slightly lower than the resonance angle of water as medium. As demonstrated in Figure 2.5 (page 91), the alternation of the layers between the adsorption of cationic sexithiophenes and anionic polycarbazole precursor resulted in the buildup of multilayers. Surface plasmon optics allow for the on-line control of film architecture while being in contact with aqueous medium. The SPS kinetic adsorption curves of 6TNL and 6TND alternating with the adsorption of PCEMMA for 10 bi-layers are shown in Figure 3.22 (a) and (b) respectively. At $t=0$, the first aqueous solution of cationic sexithiophene 6TNL or 6TND was injected into the SPS cell which charged with negatively charge functionalized gold and the adsorption followed in real time as the reflectivity changed. Each layer adsorption process of both sexithiophenes was complete after several minutes. The reflectivity increases in every layer of sexithiophenes, indicating the deposition of these sexithiophenes. After 10 minutes for sexithiophene deposition time, the film was simultaneous rinsed with water for 2 minutes as seen from the reflectivity was decreased and then stable. The negatively charged PCEMMA was then injected and allowed to adsorb for 10 minutes. The film was again rinsed with water/DMSO (2/3 v/v) for 2 minutes and then neutralized with water for further 30 seconds. The deposition procedure was repeated until the 10 bi-layers were obtained.

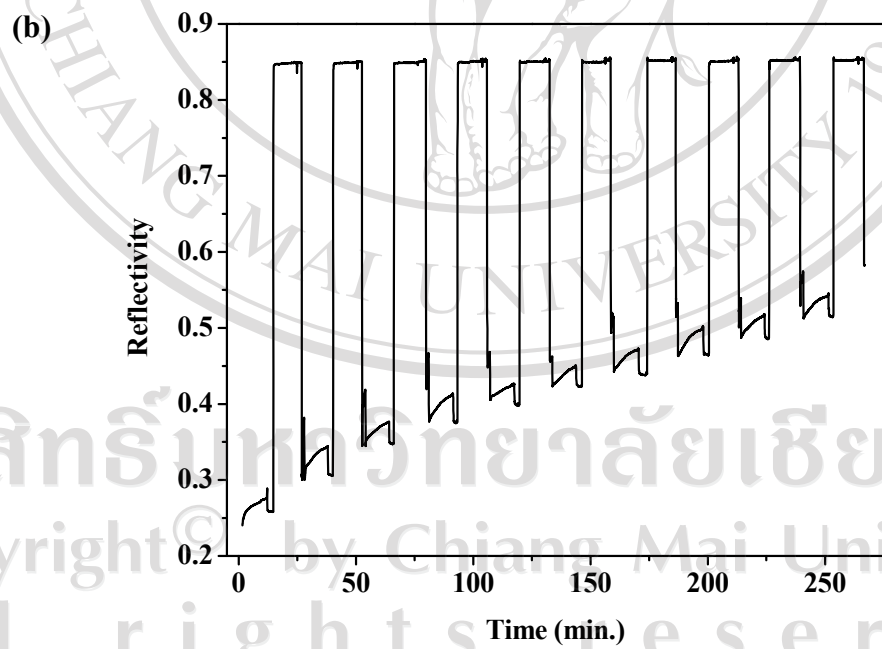
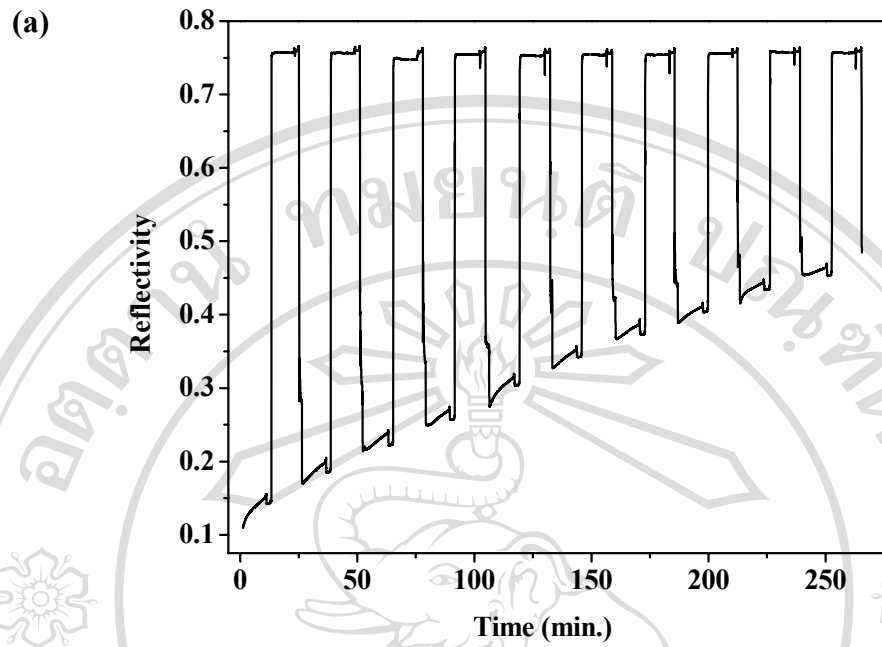


Figure 3.22 Time-dependent SPS experiment with 10 bi-layers of (a) 6TNL-PCEMMA and (b) 6TND-PCEMMA on gold-coated LaSFN9 substrate

From the kinetic curves, the reflectivity of sexithiophenes was stepwisely increased. However, for PCEMMA layer, the reflectivity was constant due to the fact that the reflectivity of DMSO/water at this fixed angle was over 0.85 as shown in Figure 3.22 (b) which will be explained later as the SPS angular scan for PCEMMA layer. Therefore, the reflectivity change could not be observed for PCEMMA layer. The angular scans were also performed before and after deposition of 10 bi-layers in water as shown in Figure 3.23. The increases in thickness were observed after 10 bi-layers for both systems.

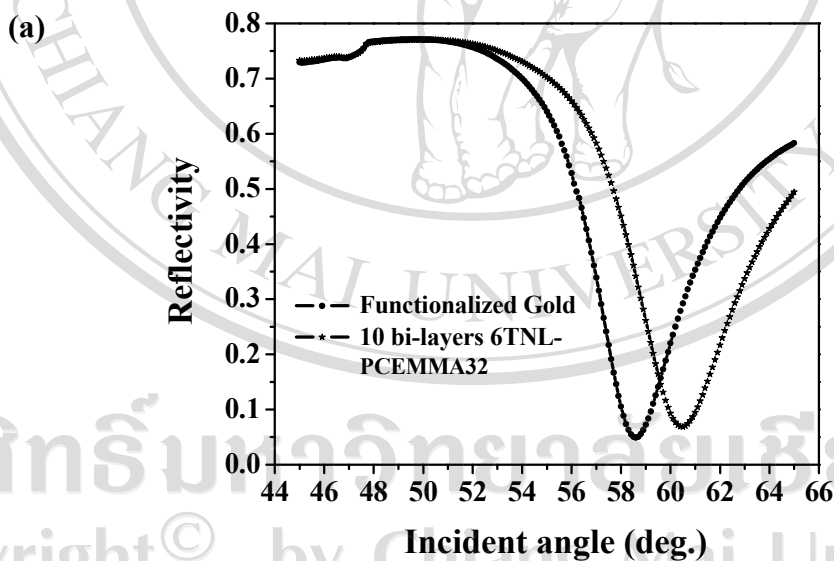


Figure 3.23 The angular measurement before and after deposition of 10 bi-layers of (a) 6TNL and (b) 6TND with PCEMMA on gold-coated LaSFN9 substrate

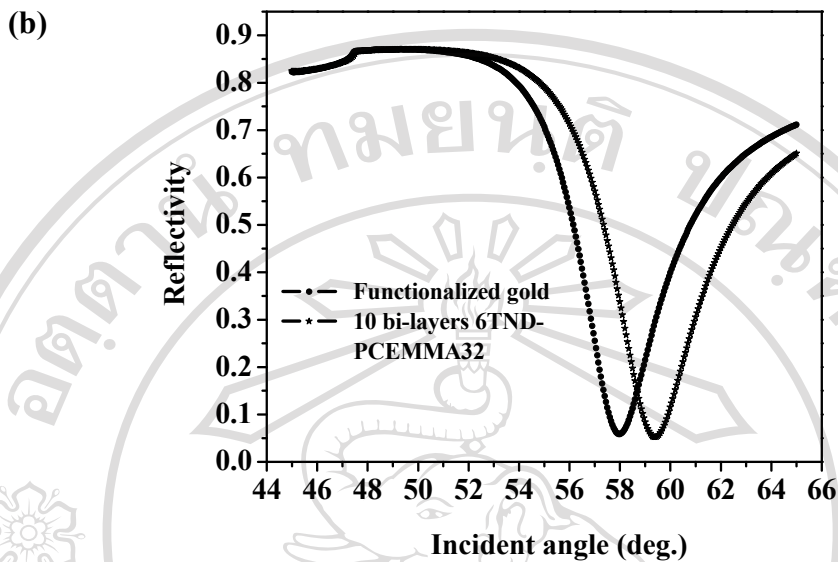


Figure 3.23 (continued)

In addition, the kinetic of adsorptions for each layer of 6TNL, 6TND and PCEMMA were also studied. The angular scans were also performed in every bi-layers deposition in water for sexithiophenes and in water/DMSO (2/3 v/v) for PCEMMA.

The reflectivity-incident angle SPS curves for 6TNL and PCEMMA system with the corresponding angular scan curves are shown in Figure 3.24 (page 146). The reflectivity-incident angle SPS curves for 6TND and PCEMMA system with the corresponding angular scan curves are shown in Figure 3.25 (page 147). Shifting of the dip angles to higher angles were observed with increasing number of layers as shown in the inset of angular scan curves.

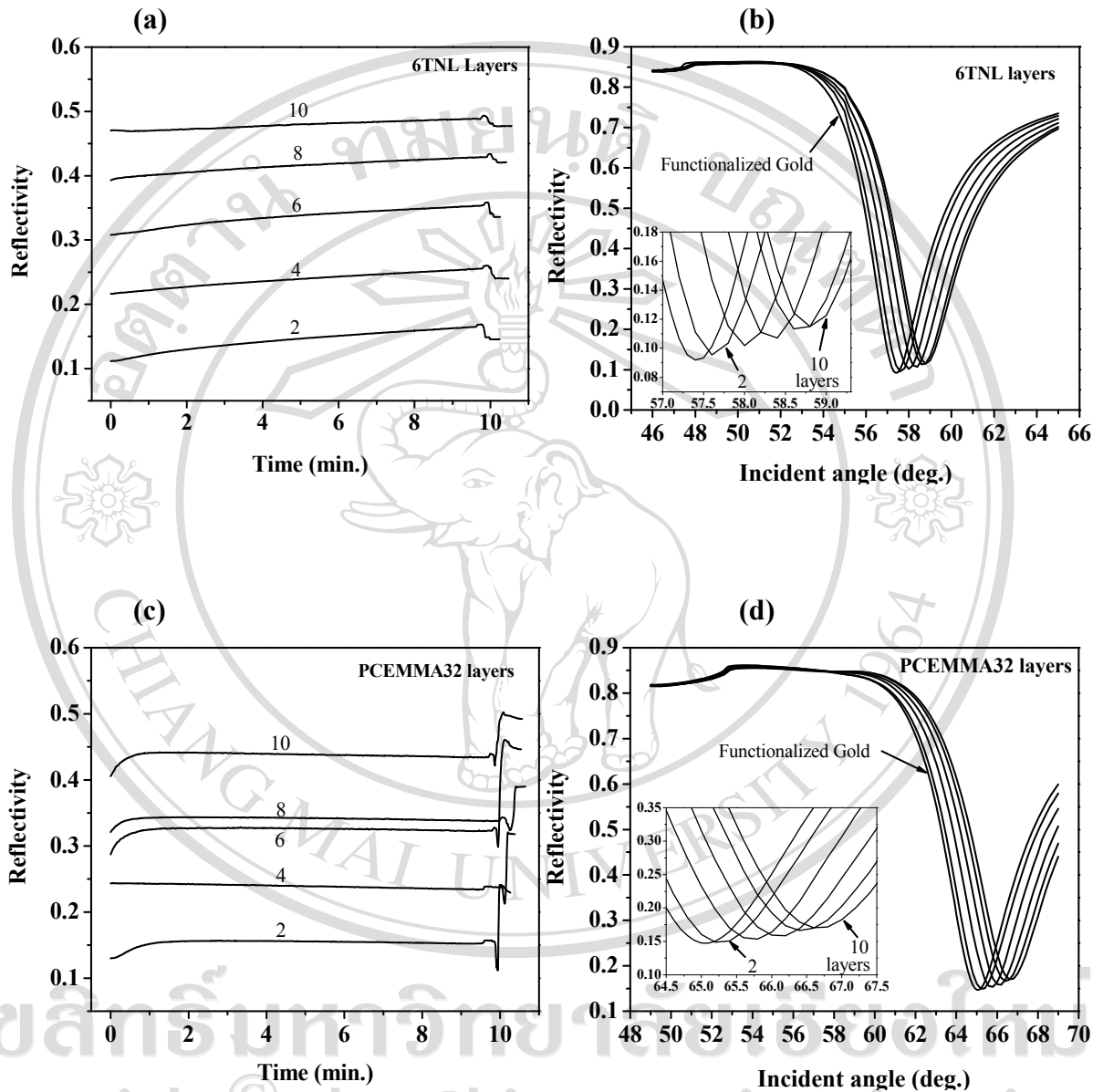


Figure 3.24 (a) Kinetic adsorption of each layer and (b) Angular scan after every 2 bi-layers deposition of 6TNL (c) Kinetic adsorption of each layer and (d) Angular scan after every 2 bi-layers deposition of PCEMMA (up to 10 bi-layers on gold-coated LaSFN9 substrate)

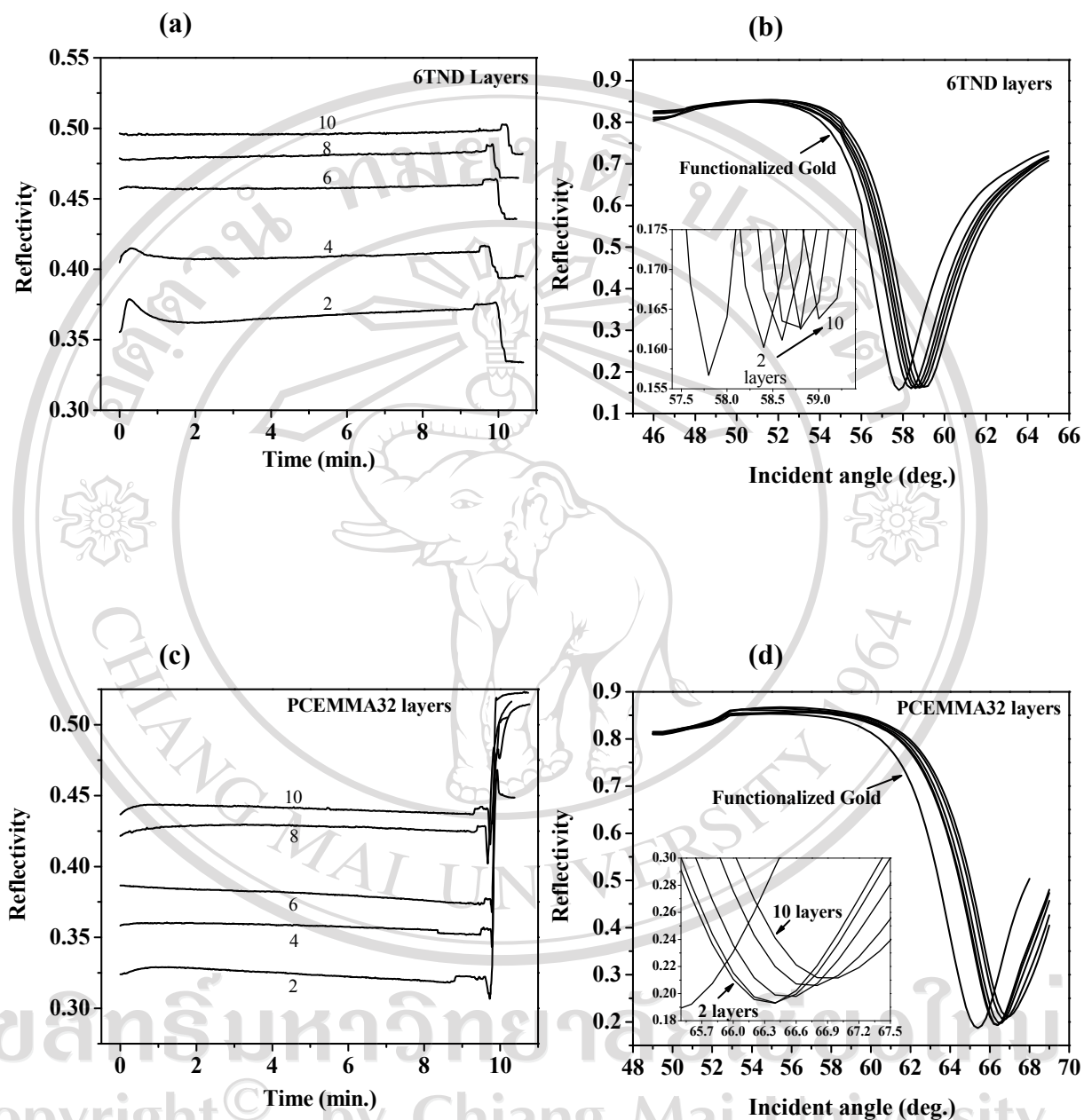


Figure 3.25 (a) Kinetic adsorption of each layer and (b) Angular scan after every 2 bi-layers deposition of 6TND (c) Kinetic adsorption of each layer and (d) Angular scan after every 2 bi-layers deposition of PCEMMA (up to 10 bi-layers on gold-coated LaSFN9 substrate)

The film thickness was calculated by fitting these experimental SPS curves with Fresnel equation using Winspall software (version 2.20). The plots of the thickness as a function of number of layers for both 6TNL and 6TND system are shown in Figure 3.26. The linearity and stepwise increasing of thickness with each layer in 6TNL system was observed which was consistent with the orderly increase in absorbance intensity as shown by UV-Vis measurement. The total film thickness was 59 Å after 10 bilayers. However, the linearity was observed after 4 bilayers in 6TND system. The total film thickness was 60 Å after 10 bilayers. It is possible that the surface charge density of each type of substrate was different. As mentioned in previous work [28, 66], the substrates were pre-deposited with 3-pair layers of polyelectrolytes (PSS/PDADMAC) to ensure the maximum surface charge density prior to deposition of their materials. The other possibility is the high charge density of 6TND (4 positive charges) which may cause the aggregation in the first-three layers. Furthermore, other studies will be required to prove the molecular orientation and morphology of the films which are considered as the important factors for device fabrication.

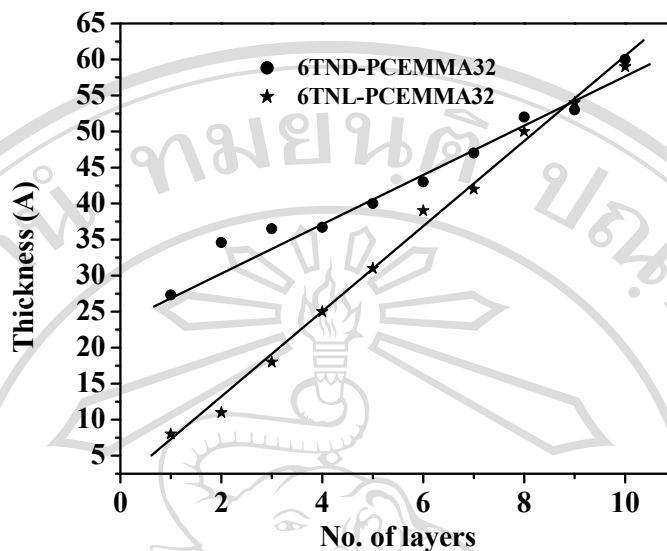


Figure 3.26 Thickness increase as a function of number of layers

3.8 Electrochemical study of multilayer films: Cyclic voltammetry

The 20 bi-layers films of both 6TNL-PCEMMA and 6TND-PCEMMA were fabricated on ITO substrates to study the electropolymerization and cross-linking of carbazole unit in PCEMMA layers. Recently, the Advincula group [21-22] studied the electropolymerization and cross-linking of poly(vinyl-*N*-carbazole) through carbazole unit as pendant side group. The CV traces of 6TNL-PCEMMA and 6TND-PCEMMA are shown in Figure 3.27 (page 151) and Figure 3.28 (page 152) respectively. The electrochemical experiment was performed in 0.1 M TBAPF₆/acetonitrile electrolyte at a scan rate of 20 mV/s. The potential was cycled from 0 to 1.4 V and 0 to 1.5 V for 10 cycles with Ag wire as a reference electrode and Pt wire as a counter electrode for both linear and dendrimeric sexithiophenes. The electrochemical process of 6TNL systems is

a reversible process, indicating that the electroactive carbazole unit is easily oxidized in 6TNL system. From the CV trace of 6TNL with potential from 0 to 1.4 V, the first cycle showed an oxidation onset peak at ~ 1.37 V and shifted to 1.4 V with the subsequent cycles. The oxidation doping peak appeared at ~ 1.16 V and shifted to ~ 1.27 V with the subsequent cycles. The appearance of this oxidation doping peak indicated the cross-linking of carbazole units in PCEMMA layers. The corresponding reduction-dedoping peak appeared at ~ 1.05 V in first cycle and shifted to ~ 1.2 V with the subsequent cycles. As for 6TNL system with potential from 0 to 1.5 V, 2 oxidation peaks were observed at ~ 1.3 and 1.5 V in first cycle. The oxidation peak at 1.5 V was still observed with subsequent cycles. The oxidation doping peak appeared at ~ 1.2 V with the corresponding reduction-dedoping peak at 1.1 V.

On the other hand, as seen in the CV trace of 6TND with potential scan from 0-1.4 V, the oxidation onset peak for the first cycle appeared at ~ 1.32 V and shifted to 1.4 V with subsequent cycles. For the potential scan from 0-1.5 V, the oxidation peak was observed at ~ 1.3 V and shifted to 1.5 V in subsequent cycles. The oxidation doping peak appeared at ~ 1.1 V with the corresponding reduction-dedoping peak at ~ 1.0 V for both potential scans. The oxidation-reduction process for 6TND was not clearly seen as obtained from cyclic voltammogram. Moreover, the significant decays of oxidation peaks were observed in the 6TND films [19]. However, the doping-dedoping currents increased with the cyclic number increased for both systems. After electropolymerization, the films were monitored with UV-Vis spectroscopy comparing with the films before electropolymerization. The UV-Vis spectra are shown in Figure 3.29 (page 153).

The carbazole peaks at ~ 330 and ~ 345 nm disappeared and the new peaks at ~ 400 nm was observed which overlapped with thiophene unit peak. The appearance of this red shift peak is due to the more conjugation of PCEMMA after electropolymerization. These results confirmed the cross-linking of carbazole unit in PCEMMA layer in both systems.

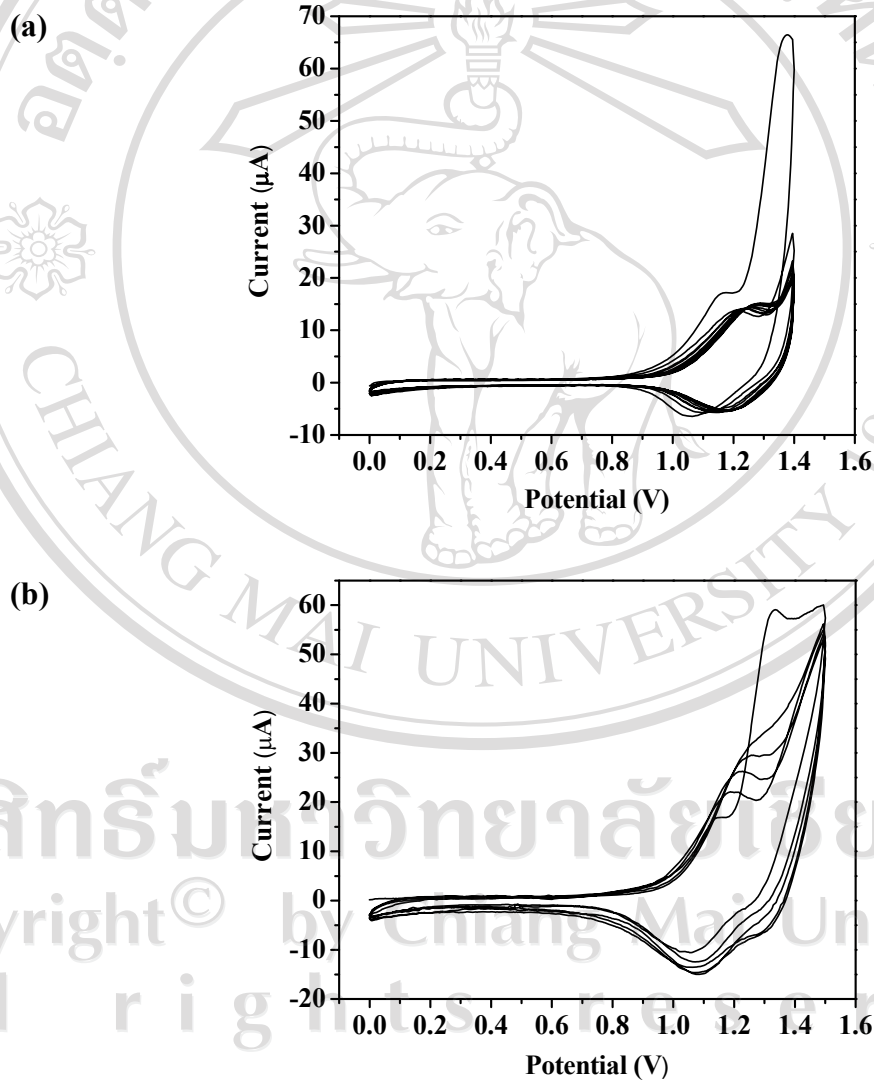


Figure 3.27 CV traces of 6TNL-PCEMMA films (20 bi-layers on ITO substrate)

with potential scan of (a) 0-1.4 V (b) 0-1.5 V

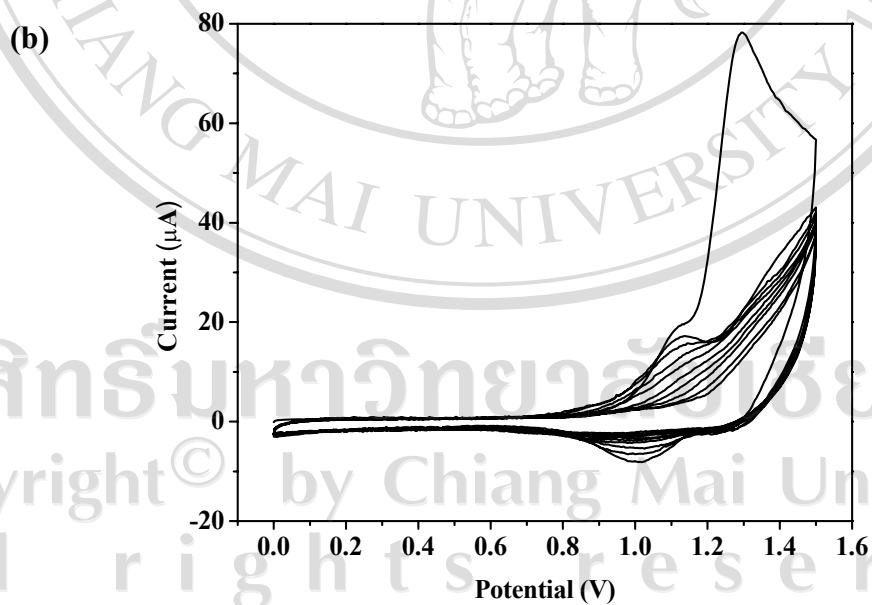
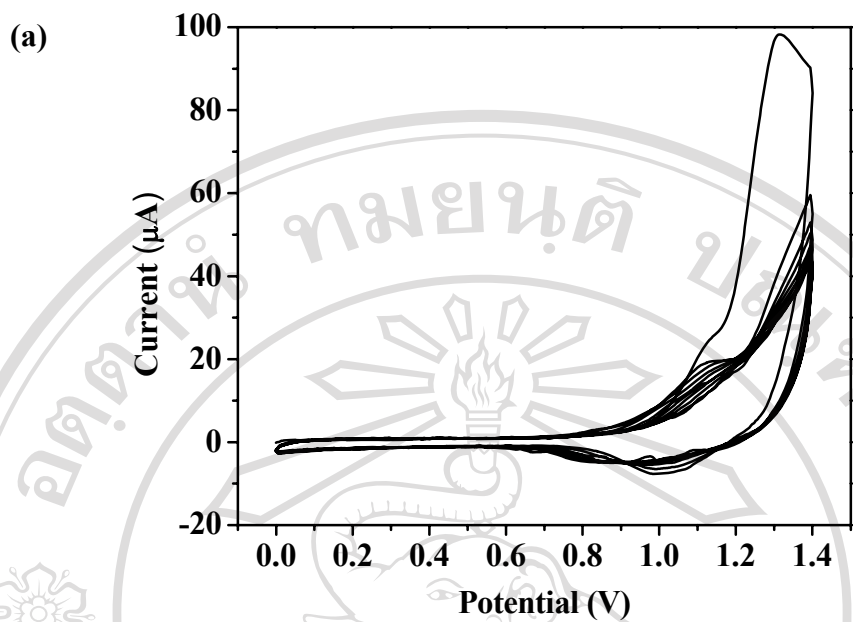


Figure 3.28 CV traces of 6TND-PCEMMA films (20 bi-layers on ITO substrate)

with potential scan of (a) 0-1.4 V (b) 0-1.5 V

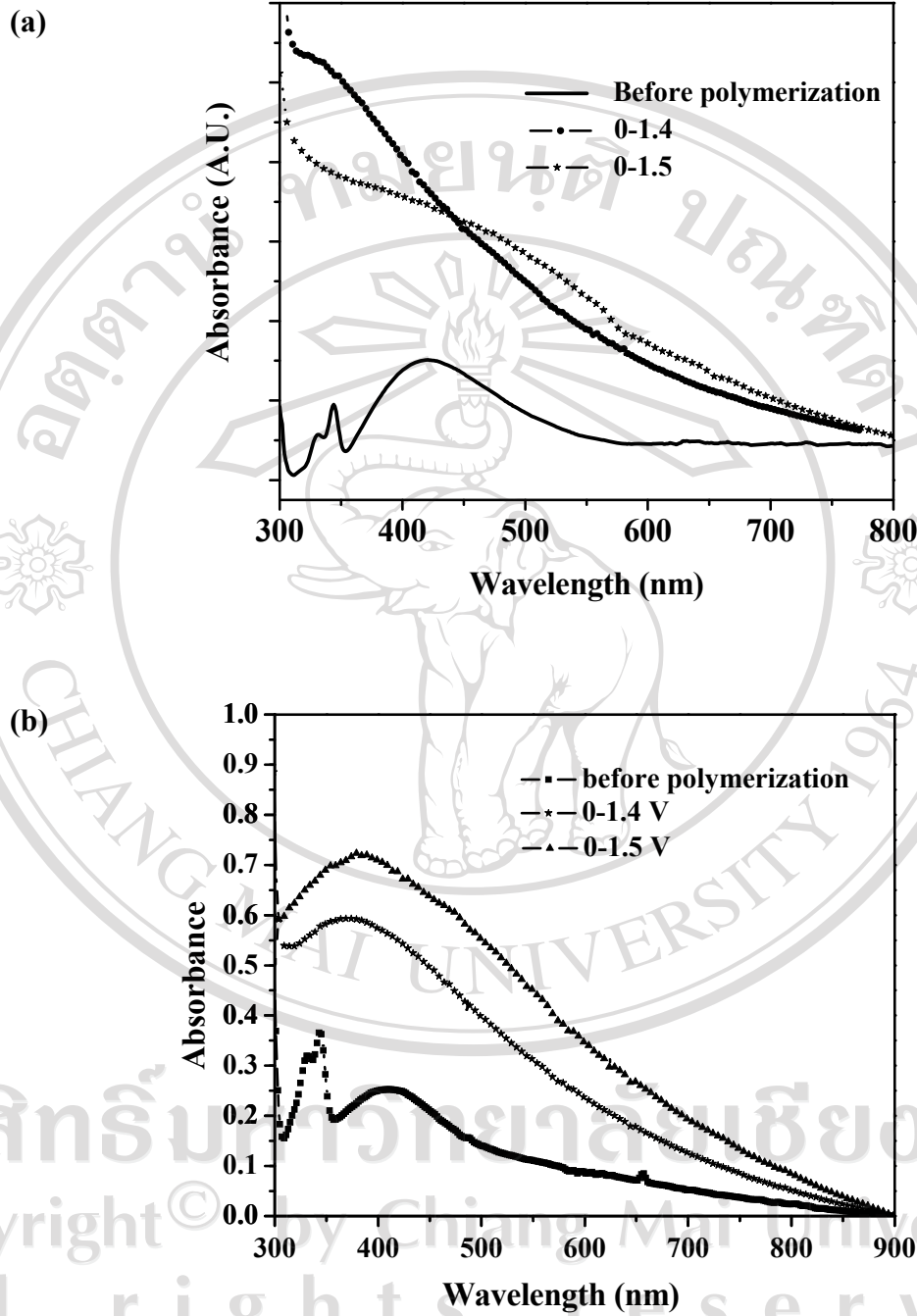


Figure 3.29 UV-Vis spectra of multilayer films taking before and after electropolymerization of (a) 6TNL-PCEMMA (b) 6TND-PCEMMA (20 bi-layers on ITO substrate)

3.9 *In situ* electrochemical investigation by EC-SPS

The combination of SPS and electrochemical method known as cyclic voltammetry (CV) had made the ability to *in situ* investigate the changes in dielectric constant and/or thickness of layer-by-layer film during the doping-dedoping or protonation-deprotonation processes [34]. The EC-SPS experiments were performed in the same condition corresponding to CV experiments. The 10 bi-layers of both systems were *in situ* fabricated on gold-coated LaSFN9 glass substrates for study the electrochemical/optical properties of the films. The kinetic of electropolymerization including potential ranges (top), amount of charge (middle) and reflectivity change (bottom) of deposited 6TNL and 6TND films are shown in Figure 3.30 (page 156) and Figure 3.31 (page 157) respectively. The data were recorded as a function of time (up to 10 cycles for 6TND and 3 cycles for 6TNL systems). The potential cycling was 0 to 1.3 V for 6TNL system and 0 to 1.2 V for 6TND system as shown in the CV traces in Figure 3.32 (a) and (b) (page 158) respectively. The stepwise increase of reflectivity was observed after each potential cycle. For 6TNL system, reflectivity in anodic scan gradually increased and then rapidly decreased at ~ 1.0 V which related to the oxidation doping peak at ~ 1.0 V as shown in CV trace. The reflectivity again increased to the maximum value at 1.3 V which corresponded to the other oxidation onset peak at 1.3 V. As increasing in number of cycle, this maximum reflectivity decreased stepwise due to the fact that the number of uncrosslinked carbazole unit in PCEMMA layer was decreased after each cycle. The rapidly increase of reflectivity was also observed in cathodic scan. On the other hand, the decrease and increase in reflectivity were observed

during the oxidation-doping and reduction-dedoping processes, respectively, of 6TND-PCEMMA film. The changes in reflectivity occurred due to the change in the dielectric constant. The amount of charge which transferred from carbazole unit to electrode for both systems showed the increase during doping process and the decrease during dedoping process as shown in the middle panel of Figure 3.30 (page 156) and Figure 3.31 (page 157) respectively. As compared the amount of charge for 6TNL and 6TND, the amount of charge of 6TNL is higher than 6TND. This means that the 6TNL gives higher level of cross-linking or doping effect. The result was again consistent with the result obtained from CV experiment. As the results of both reflectivity and amount of charge, it can be seen that 6TNL has more electrochromic property than 6TND. After the electropolymerization, the angular scans of the electropolymerized films were measured in the condition used for electropolymerization. Shifts of incident angle were observed after polymerization. As shown in Figure 3.33 (page 159), the incident angle shifted to lower angle for 6TNL film and higher angle for 6TND film. The 2 possible explanations for changing the SPS angular scan curves can be considered as follows [34, 106, 109].

The first explanation is that the thickness of films was changed after polymerization. However, if the change in thickness is the main possibility, the SPS reflectivity should increase during oxidation-doping process and decrease during reduction-dedoping process. The second explanation is that the change in the real and imaginary parts of dielectric constant of the films. Therefore, it is reasonable that the change in the dielectric constant is the primary parameter for the change in SPS reflectivity of the films.

This means the dielectric constant of the films decreases during oxidation-doping and increase during reduction-dedoping.

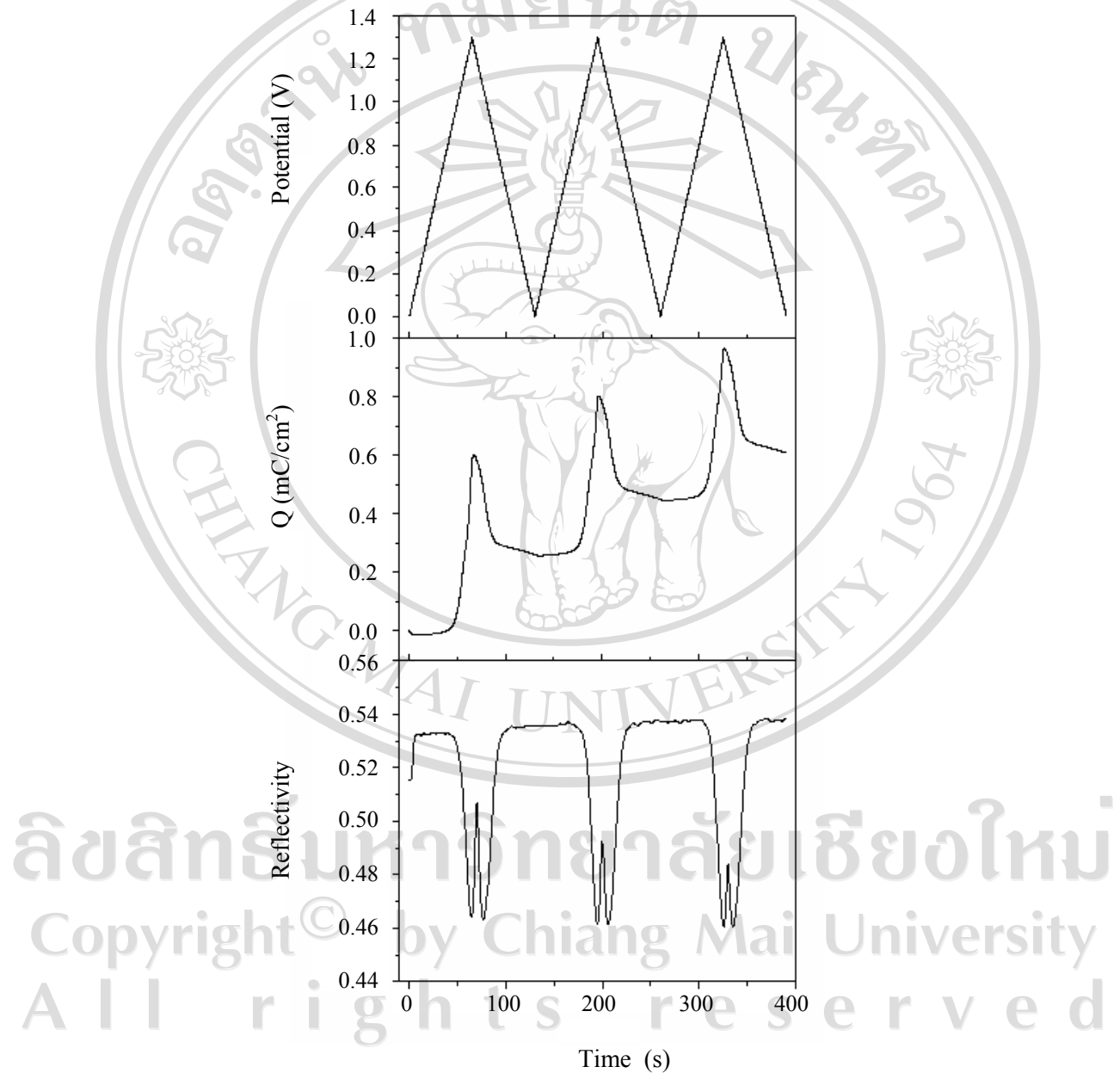


Figure 3.30 EC-SPS results of 6TNL with 10 bi-layers on gold-coated LaSFN9 substrate: potential ramp (top), amount of charge (middle) and kinetic curve (bottom)

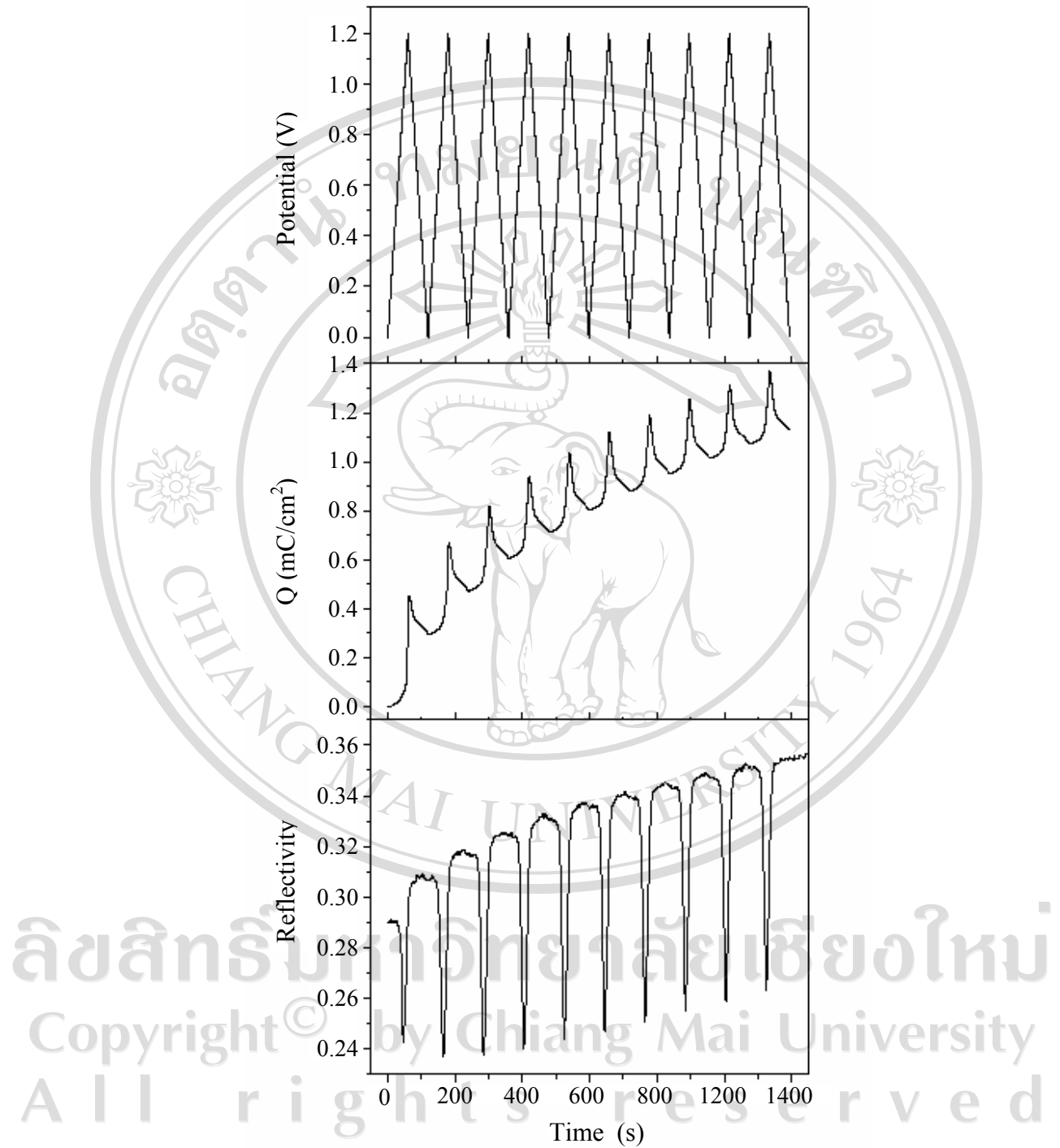


Figure 3.31 EC-SPS results of 6TND with 10 bi-layers on gold-coated LaSFN9 substrate: potential ramp (top), amount of charge (middle) and kinetic curve (bottom)

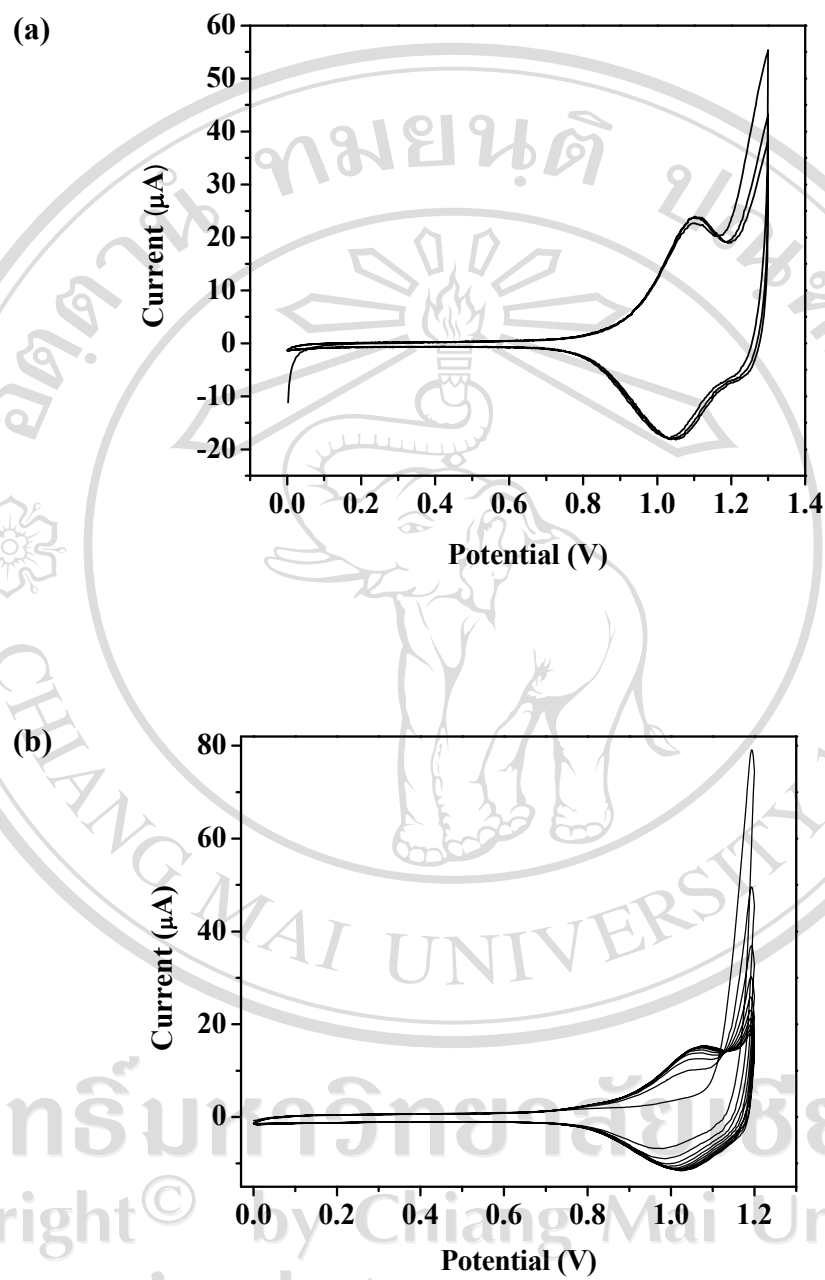


Figure 3.32 EC-SPS results: Cyclic voltammogram of (a) 6TNL and (b) 6TND

with 10 bi-layers on gold-coated LaSFN9 substrate

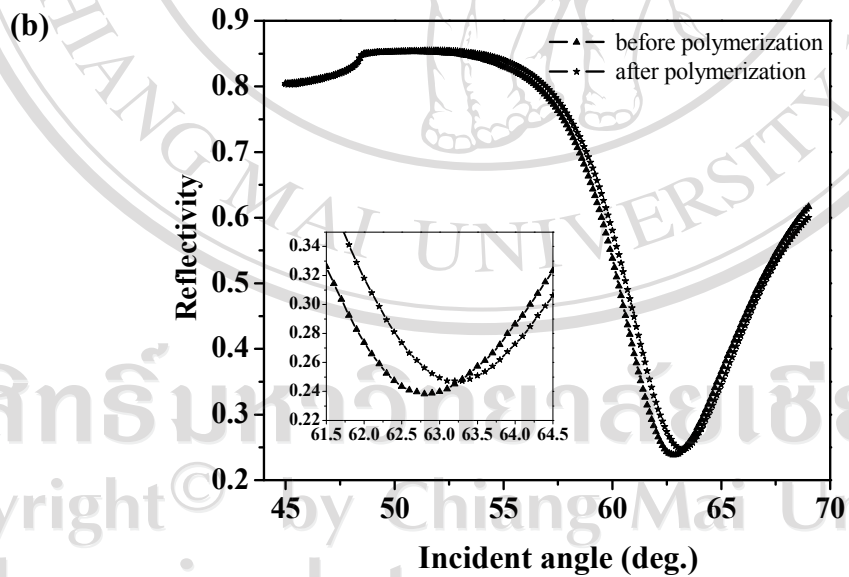
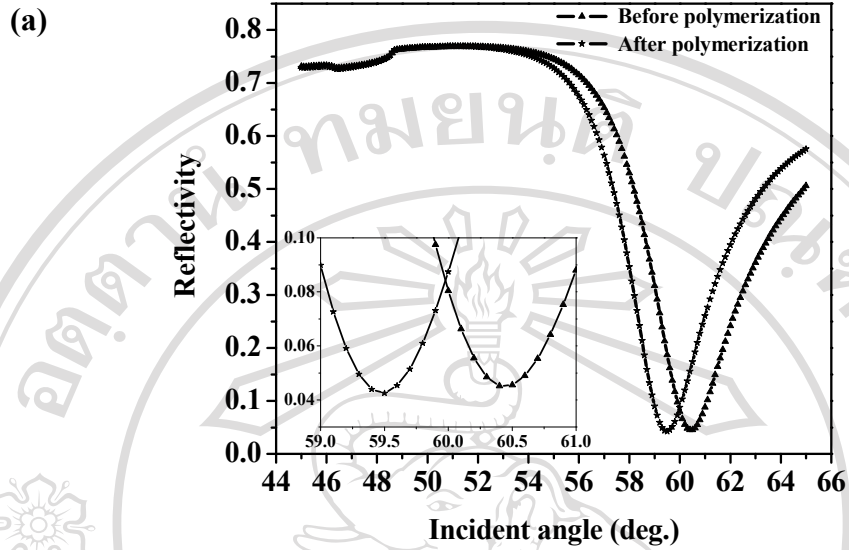


Figure 3.33 Angular scan measurement of electropolymerized films of (a) 6TNL and (b) 6TND with 10 bi-layers on gold-coated LaSFN9 substrate